



**AFRL-RZ-WP-TP-2012-0035**

**AN EXPERIMENTAL INVESTIGATION INTO THE  
TRANSIT PERFORMANCE OF A TITANIUM-WATER  
LOOP HEAT PIPE SUBJECTED TO A STEADY-PERIODIC  
ACCELERATION FIELD (POSTPRINT)**

**James D. Scofield and Kirk L. Yerkes  
Energy & Power Systems Branch**

**David L. Courson and Hua Jiang  
University of Dayton Research Institute**

**JANUARY 2012**

**Approved for public release; distribution unlimited.**

*See additional restrictions described on inside pages*

**STINFO COPY**

**AIR FORCE RESEARCH LABORATORY  
PROPULSION DIRECTORATE  
WRIGHT-PATTERSON AIR FORCE BASE, OH 45433-7251  
AIR FORCE MATERIEL COMMAND  
UNITED STATES AIR FORCE**

## NOTICE AND SIGNATURE PAGE

Using Government drawings, specifications, or other data included in this document for any purpose other than Government procurement does not in any way obligate the U.S. Government. The fact that the Government formulated or supplied the drawings, specifications, or other data does not license the holder or any other person or corporation; or convey any rights or permission to manufacture, use, or sell any patented invention that may relate to them.

This report was cleared for public release by the USAF 88<sup>th</sup> Air Base Wing (88 ABW) Public Affairs Office and is available to the general public, including foreign nationals. Copies may be obtained from the Defense Technical Information Center (DTIC) (<http://www.dtic.mil>).

AFRL-RZ-WP-TR-2012-0035 HAS BEEN REVIEWED AND IS APPROVED FOR PUBLICATION IN ACCORDANCE WITH ASSIGNED DISTRIBUTION STATEMENT.

//SIGNED//

//SIGNED//

---

JAMES SCOFIELD, Program Manager  
Energy & Power Systems Branch  
Energy/Power/Thermal Division

---

JOSEPH A. WEIMER, Branch Chief  
Energy & Power Systems Branch  
Energy/Power/Thermal Division

This report is published in the interest of scientific and technical information exchange, and its publication does not constitute the Government's approval or disapproval of its ideas or findings.

\*Disseminated copies will show “//signature//” stamped or typed above the signature blocks.

<b>REPORT DOCUMENTATION PAGE</b>					<i>Form Approved</i> OMB No. 0704-0188	
The public reporting burden for this collection of information is estimated to average 1 hour per response, including the time for reviewing instructions, searching existing data sources, gathering and maintaining the data needed, and completing and reviewing the collection of information. Send comments regarding this burden estimate or any other aspect of this collection of information, including suggestions for reducing this burden, to Department of Defense, Washington Headquarters Services, Directorate for Information Operations and Reports (0704-0188), 1215 Jefferson Davis Highway, Suite 1204, Arlington, VA 22202-4302. Respondents should be aware that notwithstanding any other provision of law, no person shall be subject to any penalty for failing to comply with a collection of information if it does not display a currently valid OMB control number. <b>PLEASE DO NOT RETURN YOUR FORM TO THE ABOVE ADDRESS.</b>						
<b>1. REPORT DATE (DD-MM-YY)</b> February 2012		<b>2. REPORT TYPE</b> Technical Paper		<b>3. DATES COVERED (From - To)</b> 1 September 2010 – 1 July 2011		
<b>4. TITLE AND SUBTITLE</b> AN EXPERIMENTAL INVESTIGATION INTO THE TRANSIT PERFORMANCE OF A TITANIUM-WATER LOOP HEAT PIPE SUBJECTED TO A STEADY-PERIODIC ACCELERATION FIELD (POSTPRINT)				<b>5a. CONTRACT NUMBER</b> In-house		
				<b>5b. GRANT NUMBER</b>		
				<b>5c. PROGRAM ELEMENT NUMBER</b> 62203F		
<b>6. AUTHOR(S)</b> James Scofield and Kirk L. Yerkes (AFRL/RZPE) David L. Courson and Hua Jiang (University of Dayton Research Institute)				<b>5d. PROJECT NUMBER</b> 3145		
				<b>5e. TASK NUMBER</b> 13		
				<b>5f. WORK UNIT NUMBER</b> 31451311		
<b>7. PERFORMING ORGANIZATION NAME(S) AND ADDRESS(ES)</b> Energy and Power Systems Branch (AFRL/RZPE) Air Force Research Laboratory, Propulsion Directorate Wright-Patterson Air Force Base, OH 45433-7251 Air Force Materiel Command, United States Air Force				University of Dayton Research Institute 300 College Park Avenue Dayton, OH 45469		
<b>9. SPONSORING/MONITORING AGENCY NAME(S) AND ADDRESS(ES)</b> Air Force Research Laboratory Propulsion Directorate Wright-Patterson Air Force Base, OH 45433-7251 Air Force Materiel Command United States Air Force				<b>10. SPONSORING/MONITORING AGENCY ACRONYM(S)</b> AFRL/RZPE		
				<b>11. SPONSORING/MONITORING AGENCY REPORT NUMBER(S)</b> AFRL-RZ-WP-TP-2012-0035		
<b>12. DISTRIBUTION/AVAILABILITY STATEMENT</b> Approved for public release; distribution unlimited.						
<b>13. SUPPLEMENTARY NOTES</b> The U.S. Government is joint author of this work and has the right to use, modify, reproduce, release, perform, display, or disclose the work. PA Case Number and clearance date: 88ABW-2011-6151, 05 Jan 2012. Postprint journal article published in Proceedings AIAA (2012-1009), Aerospace Sciences Meeting, 9-12 January 2012, Nashville, Tennessee. This document contains color.						
<b>14. ABSTRACT</b> The objective of this research is to experimentally investigate the transient operating characteristics of a titanium-water loop heat pipe subjected to a combined steady-state evaporator input heat rate and a steady-periodic acceleration field. For this experimental investigation, a steady-periodic acceleration field, in the form of a sine wave, was generated using a centrifuge table. Radial acceleration peak-to-peak values and frequency of the sine wave were defined prior to conducting each experimental run and ranged from $0.5g \leq a_r \leq 10g$ , and $0.01Hz \leq f \leq 0.1Hz$ respectively. Evaporator input heat rate and condenser cold plate coolant temperature was varied $300W \leq Q_{in} \leq 600W$ and $30oC \leq T_{cp} \leq 56oC$ respectively. In some cases acceleration driven forces complimented the thermodynamic forces improving LHP dynamical performance. However, the converse was also true in that transient acceleration driven forces also appeared to counter thermodynamic forces or excite natural frequencies of the LHP. This resulted in immediate total failure of the LHP to operate, delayed total failure, or in some cases, the LHP operated in a stable manner but in a degraded condition.						
<b>15. SUBJECT TERMS</b> loop heat pipe, body force, centrifuge testing, acceleration transients						
<b>16. SECURITY CLASSIFICATION OF:</b>			<b>17. LIMITATION OF ABSTRACT:</b> SAR	<b>NUMBER OF PAGES</b> 40	<b>19a. NAME OF RESPONSIBLE PERSON (Monitor)</b> James Scofield	
<b>a. REPORT</b> Unclassified	<b>b. ABSTRACT</b> Unclassified	<b>c. THIS PAGE</b> Unclassified			<b>19b. TELEPHONE NUMBER (Include Area Code)</b> N/A	

# **An Experimental Investigation into the Transient Performance of a Titanium-Water Loop Heat Pipe Subjected to a Steady-Periodic Acceleration Field**

Kirk L. Yerkes<sup>1</sup> and James D. Scofield<sup>2</sup>

*U.S. Air force Research Laboratory, Wright-Patterson Air Force Base, Ohio 45433*

David L. Courson<sup>3</sup> and Hua Jiang<sup>4</sup>

*University of Dayton Research Institute, Dayton, Ohio 45469*

The objective of this research is to experimentally investigate the transient operating characteristics of a titanium-water loop heat pipe subjected to a combined steady-state evaporator input heat rate and a steady-periodic acceleration field. For this experimental investigation, a steady-periodic acceleration field, in the form of a sine wave, was generated using a centrifuge table. Radial acceleration peak-to-peak values and frequency of the sine wave were defined prior to conducting each experimental run and ranged from  $0.5g \leq a_r \leq 10g$ , and  $0.01Hz \leq f \leq 0.1Hz$  respectively. Evaporator input heat rate and condenser cold plate coolant temperature was varied  $300W \leq Q_{in} \leq 600W$  and  $30^\circ C \leq T_{cp} \leq 56^\circ C$  respectively. In some cases acceleration driven forces complimented the thermodynamic forces improving LHP dynamical performance. However, the converse was also true in that transient acceleration driven forces also appeared to counter thermodynamic forces or excite natural frequencies of the LHP. This resulted in immediate total failure of the LHP to operate, delayed total failure, or in some cases, the LHP operated in a stable manner but in a degraded condition.

<sup>1</sup>Energy Science and Integration Research Advisor, Propulsion Directorate, AFRL/RZPE, Wright-Patterson AFB, Ohio 45433, Associate Fellow

<sup>2</sup>Power Electronics CTC Lead, Propulsion Directorate, AFRL/RZPE, Wright-Patterson AFB, Ohio 45433

<sup>3</sup>Associate Research Engineer, Energy, Technologies & Materials Division, University of Dayton Research Institute, Dayton, Ohio 45469

<sup>4</sup>Thermal Scientist, Energy, Technologies & Materials Division, University of Dayton Research Institute, Dayton, Ohio 45469

## Nomenclature

$\mathbf{a}_{eff}$	effective acceleration vector field on the LHP
ar	radial acceleration component, g
at	tangential acceleration component, g
az	vertical acceleration component, g
$\hat{\mathbf{e}}$	coordinate axis unit vector
f	acceleration frequency, Hz
$\mathbf{g}$	acceleration vector due to gravity
$g$	acceleration vertical component due to gravity, g
Q	heat rate, W
Q <sub>in</sub>	input heat rate, W
$\mathbf{r}$	position vector
r	position vector radial coordinate, m
$R_{ref}$	reference position; accelerometer radial position, 1.208m (47.56in)
$r_1$	LHP condenser end radial location, 1.219m (48.0in)
$r_2$	LHP condenser end radial location, 1.215m (47.82in)
t	time, min or sec
T	temperature, °C
T <sub>cp</sub>	cold plate coolant inlet temperature, °C
$z_r$	position vector vertical coordinate, m

## Greek

$\theta$	angular position of the position vector, degrees
$\theta_1$	angular position of the position vector at $r_1$ , 0°
$\theta_2$	angular position of the position vector at $r_2$ , 16.82°
$\boldsymbol{\omega}$	angular velocity vector
$\omega$	angular velocity vector component, rad/sec

**Subscripts**

$r_{LHP}$  radial component of the acceleration vector oriented on the LHP

$y_{LHP}$  radial component of the acceleration vector oriented with the accelerometer

$x_{LHP}$  tangential component of the acceleration vector oriented with the accelerometer

$z$  vertical component of the acceleration vector

$z_{LHP}$  axial component of the acceleration vector oriented on the LHP

## I. Introduction

The loop heat pipe (LHP), due to its passive heat transport capability, is one potential solution for a variety of aircraft thermal management challenges such as cooling power electronics components. At best, the LHP represents the transport of heat due to the complex interaction of numerous thermodynamics forces<sup>1</sup>. Its operation can embody a variety of dynamical responses when perturbed by driving forces such as evaporator input heat rate load and temperatures of the condenser and compensation chamber<sup>2</sup>. This dynamical behavior can introduce either long-term low frequency oscillations or short-term dynamics leading to instabilities resulting in LHP failure. These oscillations during LHP operation have been observed experimentally, however, the physics-based modeling of the dynamical performance and stability criterion of a LHP has been limited<sup>3-7</sup>. In addition, the LHP can also be sensitive to external body forces, such as transitory acceleration induced forces, that may alter the LHP dynamical performance and stability. Typically, the LHP has been assumed to be insensitive to acceleration induced forces due to the design and wicking properties of the discrete capillary structure within the evaporator. Ku<sup>8,9</sup> studied the effect of the acceleration induced forces on the LHP operating temperatures. When a centrifugal force was applied to the LHP, it was found that steady-state acceleration induced forces altered liquid/vapor distributions within the LHP which significantly influenced its performance and temperature oscillation.

Fleming et al.<sup>10</sup> investigated the steady-state performance of a titanium-water LHP mounted on a centrifuge and subjected to elevated acceleration. These preliminary experimental investigations defined the steady-state operating characteristics of the LHP subjected to a combined steady-state input heat rate and steady-state acceleration field. It was observed that the position of the liquid/vapor interface in the condenser was influenced by steady-state acceleration induced forces. This either limited or enhanced condenser performance depending upon the extent to which the liquid/vapor interface closed or opened up the condenser to allow the condensation process to occur. As a result of poor condenser performance, the evaporator wick unexpectedly dried out at a relative lower input heat with low acceleration. However, with an increased input heat rate, >500 W, the condenser performance improved resulting in a steady-state operation for a radial acceleration up to 10g. It was believed that this reverse behavior is associated with a nonlinear coupling of thermodynamic induced forces with the acceleration induced forces within the condenser.

The physical meaning of and subsequent LHP performance resulting from acceleration induced forces on the condenser operation is not well understood. It is suspected that with combined heat input and elevated acceleration,

competing thermodynamic forces and steady-state acceleration induced forces must balance allowing the LHP to either operate or fail. At best, the “normal” performance of a LHP involves complex coupled thermodynamics associated with fluid thermal properties and thermodynamic forces throughout the LHP. In an accelerating environment, steady-state or transitory, the prediction of LHP performance is difficult without a thorough understanding as to the nature of competing or complementing thermodynamic induced forces with acceleration induced forces across the entire LHP.

This study experimentally investigates the effect of a steady-periodic acceleration field, in the form of a sine wave, on the performance of the LHP. Specifically, the initial transient behavior of the LHP due to a step-increase in heat input and the steady-periodic behavior due to a steady-periodic acceleration are investigated. In addition, a series of time-dependent acceleration equations were derived which relate the time-variant directionality of the acceleration vector field to the time-variant directionality of the acceleration induced force field. Thus, the thermodynamic induced forces can be compared with the acceleration induced force distribution across the LHP.

## **II. Experimental Approach**

Figure 1 schematically shows the experimental apparatus consisting of a 2.44-m horizontal centrifuge table and a titanium-water LHP. Figures 1a show the centrifuge table, data acquisition system, accelerometer, rotary hydraulic coupling, and cool bath used for the experiments. Power and instrumentation signals were passed through separated rotational slip rings to minimize electrical noise and interference. Transient acceleration measurements were made using a rectangular coordinate system orthogonal triaxial Columbia (model SA-307HPTX) accelerometer with an uncertainty of  $\pm 0.01g$ . The accelerometer was mounted such that the radial acceleration component was aligned with y-axis. The accelerometer output was consistent with a right-hand coordinate system with the y-axis and x-axis mounted in the radial direction and the tangential direction respectively. To ensure proper control of the centrifuge table during the experiments, radial acceleration profiles were digitally generated, stored on a Fluke Waveform Generator (Model 292), and integrated into a LabView data acquisition and control program for the centrifuge table.

For this experimental investigation, an intermediate water coolant loop supplied coolant to the cold plate heat sink mounted to the LHP condenser. A Tek Temp cool bath, consisting of a pump, reservoir, and liquid-air heat exchanger, was operated external to the centrifuge in order to provide sufficient temperature control of the water coolant to maintain the cold plate inlet temperature,  $T_{cp}$ . Water coolant flow, from the cool bath, was supplied to the



centrifuge through the use of a rotating hydraulic slip ring. The cold plate coolant flow rate was measured and maintained at 0.077kg/s, with an uncertainty to within 5%, using a calibrated Sponsler (model SP 711-3) flow meter mounted on the centrifuge table. Figure 1b schematically illustrates the titanium-water LHP and thermocouple locations monitored during the experiments. The LHP was fabricated by Advanced Cooling Technologies (ACT) Inc as discussed in detail by Fleming et.al. To reduce ambient temperature effects and minimize system heat loss, the LHP was insulated with overlapping (multiple) layers of ½” FiberFrax<sup>®</sup> with an outer layer of aluminum foil. The entire LHP is enclosed within an additional aluminum sheet metal skin covering a 80/20 support framework.

Temperature measurements were made using both calibrated type-T and type-E thermocouples with an uncertainty of approximately  $\pm 0.05^{\circ}\text{C}$ . All of the low voltage thermocouple outputs were preconditioned and amplified on the centrifuge to minimize losses through the instrumentation slip ring. Bare thermocouple beads were mounted in place with thermal grease and secured with Kapton tape.

The evaporator input heat rate to the LHP was provided using a mica heater (Minco) mounted on the evaporator and powered from the output of a Kepco (model ATE-150-7M) power supply. Evaporator heater power was determined from voltage measurements across a precision resistor, in series with the evaporator heater, with an uncertainty of  $\sim 2.0\%$ .

During the LHP operation, the compensation chamber was insulated without additional heating or cooling. Thermocouples were mounted around the centerline circumference of the compensation chamber to measure any temperature variation as a result of fluid slosh due to induced accelerations. The LHP was mounted in such a manner as to minimize the radial variation along the length of the LHP. The vapor and liquid lines were bent to maintain the radius of curvature of the centrifuge. However, the condenser/cold plate and evaporator/compensation chamber varied in radial location due to their linear construction. This introduced an acceleration gradient along the length of the condenser/cold plate and evaporator/compensation chamber.

### III. Acceleration Vector Field

Figure 1c shows the centrifuge coordinate system and the condenser mounting position used to derive the position vector and subsequently the vector form of the acceleration field across the condenser. To align the right-handed coordinate system,  $\hat{e}_x, \hat{e}_y, \hat{e}_z$ , with the accelerometer right-handed coordinate system,  $\hat{e}_{xLHP}, \hat{e}_{yLHP}, \hat{e}_z$ , it is rotated clockwise to align the radial acceleration component,  $r$ , with the y-axis of both coordinate systems. The

linear region bounded by  $(r_1, \theta_1)$  and  $(r_2, \theta_2)$  represents the tubular condenser region of the loop heat pipe. The position vector,  $\mathbf{r}$ , is bounded by this linear condenser region and can be described and formulated in rectangular coordinates by

$$\mathbf{r} = r\hat{\mathbf{e}}_{y_{LHP}} + z_r\hat{\mathbf{e}}_z. \quad (1)$$

The component,  $r$ , can easily be transformed in terms of  $\theta$  where the linear portion of the condenser can be described as

$$y_r = ax_r + b, \quad (2)$$

where

$$x_r = r \cos \theta, \text{ and } y_r = r \sin \theta. \quad (3)$$

In terms of  $r_1$ ,  $r_2$ , and  $\theta_2$ ;

$$a = \frac{r_2 \sin \theta_2}{r_2 \cos \theta_2 - r_1}$$

and

$$b = -\frac{r_1 r_2 \sin \theta_2}{r_2 \cos \theta_2 - r_1}.$$

Substituting Eqn. (3) into Eqn. (2);

$$y_r = r \sin \theta = \frac{(r_2 \sin \theta_2)(r_1 - r \cos \theta)}{(r_1 - r_2 \cos \theta_2)},$$

where the radial component,  $r$ , can be shown to be

$$r = \frac{r_1}{\left( \frac{(\sin \theta)(r_1 - r_2 \cos \theta_2)}{(r_2 \sin \theta_2)} + \cos \theta \right)}. \quad (4)$$

The position vector can now be written as

$$\mathbf{r} = \left( \frac{r_1}{\left( \frac{(\sin \theta)(r_1 - r_2 \cos \theta_2)}{(r_2 \sin \theta_2)} + \cos \theta \right)} \right) \hat{\mathbf{e}}_{y_{LHP}} + z_r \hat{\mathbf{e}}_z, \quad (5)$$

where

$$\theta_1 \leq \theta \leq \theta_2.$$

The effective acceleration vector field on the LHP becomes

$$\mathbf{a}_{eff} = \frac{d^2 \mathbf{r}}{dt^2} = \mathbf{g} + \left[ \left( 2\boldsymbol{\omega} \times \frac{d\mathbf{r}}{dt} \right) + \left( \frac{d\boldsymbol{\omega}}{dt} \times \mathbf{r} \right) + \boldsymbol{\omega} \times (\boldsymbol{\omega} \times \mathbf{r}) \right], \quad (6)$$

where  $\mathbf{g} = -g\hat{\mathbf{e}}_z$  represents acceleration due to gravity. With the LHP being affixed to the centrifuge table,

$$\frac{d\mathbf{r}}{dt} = 0,$$

$$\mathbf{a}_{eff} = \mathbf{g} + \left[ \left( \frac{d\boldsymbol{\omega}}{dt} \times \mathbf{r} \right) + \boldsymbol{\omega} \times (\boldsymbol{\omega} \times \mathbf{r}) \right]. \quad (7)$$

For these experiments, the radial acceleration is controlled as a sine wave of the form of an offset sine wave,  $\omega^2 R_{ref} = A \sin 2\pi ft + B$ . Accounting for the clockwise rotation of the centrifuge, the angular velocity vector becomes

$$\boldsymbol{\omega} = -\omega \hat{\mathbf{e}}_z = -\sqrt{\frac{(A \sin 2\pi ft + B)}{R_{ref}}} \hat{\mathbf{e}}_z, \quad (8)$$

where

$$A = \left( \frac{ar_{high} - ar_{low}}{2} \right),$$

$$B = \left( \frac{ar_{high} + ar_{low}}{2} \right),$$

and

$$\frac{d\boldsymbol{\omega}}{dt} = -\frac{A\pi f \cos 2\pi ft}{\sqrt{R_{ref} (A \sin 2\pi ft + B)}} \hat{\mathbf{e}}_z \quad (9)$$

The cross products in Eqn. (7) can now be evaluated where the final form of the effective acceleration vector field, at any given point on the LHP as defined by  $\theta$ , now becomes

$$\begin{aligned} \mathbf{a}_{eff} &= at\hat{\mathbf{e}}_{xLHP} + ar\hat{\mathbf{e}}_{yLHP} + az\hat{\mathbf{e}}_z = r\frac{d\omega}{dt}\hat{\mathbf{e}}_{xLHP} + r(-\omega)^2\hat{\mathbf{e}}_{yLHP} + (-g)\hat{\mathbf{e}}_z \\ &= \left\{ \left( \frac{r_1}{\left( \frac{(\sin \theta)(r_1 - r_2 \cos \theta_2)}{(r_2 \sin \theta_2)} + \cos \theta \right)} \right) \left( -\frac{A\pi f \cos 2\pi ft}{\sqrt{R_{ref} (A \sin 2\pi ft + B)}} \right) \right\} \hat{\mathbf{e}}_{xLHP} \\ &\quad + \left\{ \left( \frac{(A \sin 2\pi ft + B)}{R_{ref}} \right) \left( \frac{r_1}{\left( \frac{(\sin \theta)(r_1 - r_2 \cos \theta_2)}{(r_2 \sin \theta_2)} + \cos \theta \right)} \right) \right\} \hat{\mathbf{e}}_{yLHP} \\ &\quad + (-g)\hat{\mathbf{e}}_z. \end{aligned} \quad (10)$$

To determine acceleration field within the LHP, the coordinate system  $\hat{\mathbf{e}}_{xLHP}, \hat{\mathbf{e}}_{yLHP}, \hat{\mathbf{e}}_z$ , as shown by Eqn. 10, can be rotated to align with the radial and axial coordinates,  $\hat{\mathbf{e}}_{rLHP}, \hat{\mathbf{e}}_{zLHP}, \hat{\mathbf{e}}_z$ , of the LHP, Fig. 2. (Note, the radial

acceleration component as described is really a transverse acceleration component generated by a combination of the radial and tangential acceleration of the centrifuge. For this discussion, this component is acting normal to the centerline of the LHP.) Now from Eqn.10,

$$\mathbf{a}_{eff} = at\hat{\mathbf{e}}_{xLHP} + ar\hat{\mathbf{e}}_{yLHP} + az\hat{\mathbf{e}}_z = a_{zLHP}\hat{\mathbf{e}}_{zLHP} + a_{rLHP}\hat{\mathbf{e}}_{rLHP} + (-g)\hat{\mathbf{e}}_z$$

for the case where  $\varphi < 90^\circ$  and  $\beta = (90^\circ - \varphi)$ ;

$$a_{zLHP} = (ar \sin \beta + at \cos \beta)$$

and

$$a_{rLHP} = (ar \cos \beta - at \sin \beta).$$

Similarly, where  $\varphi > 90^\circ$  and  $\beta = (\varphi - 90^\circ)$ ;

$$a_{zLHP} = (at \cos \beta - ar \sin \beta)$$

and

$$a_{rLHP} = (at \sin \beta + ar \cos \beta).$$

The angle  $\varphi$  can be determined by the relationship

$$\varphi = (\theta + \varphi_1),$$

where

$$\varphi_1 = \sin^{-1} \left( \frac{r_2 \sin \theta_2}{L} \right).$$

Figure 3 shows the acceleration components; axial,  $a_{zLHP}$ , and radial,  $a_{rLHP}$ , referenced to the LHP condenser for varying position vector angle,  $\theta$ . Comparing the two endpoint cases at  $r_1$  and  $r_2$  where  $\theta = \theta_1 = 0^\circ$  and  $\theta = \theta_2 = 16.82^\circ$  respectively, the axial acceleration components at the condenser ends are acting in opposite and outward directions with a maximum magnitude up to  $\sim 1.5g$ . The axial acceleration component located at the  $r_1$  position is slight greater which is consistent with the fact that  $r_1 > r_2$ . This may contribute to additional acceleration-driven pumping forces due to acceleration gradients down the length of the condenser during the LHP operation. It must also be noted that while the radial and transverse acceleration components remain consistent with the transitory radial acceleration generated by the centrifuge, the vertical acceleration component due to gravity also contributes and remains constant,  $az = -g$ .

#### IV. Results and Discussion

Figure 4 compares experimental to calculated acceleration where  $\theta = 14^\circ$ ,  $f = 0.05\text{Hz}$ , and  $1.0g \leq ar \leq 10.0g$ . At the angular position of  $\theta = 14^\circ$  the effective radius,  $R_{ref} = 1.208\text{m}$  (47.56in), is the same for both the accelerometer

and the LHP radial position. Figure 4a shows the radial and tangential acceleration components obtained from the experimental accelerometer. The tangential component was determined using the rate of change of radial acceleration,  $a_r$ , to calculate the tangential acceleration component

$$a_t = r \frac{d\sqrt{a_r/r}}{dt} \cong r \frac{\Delta\sqrt{a_r/r}}{\Delta t}.$$

Figure 4b shows the corresponding acceleration calculated using Eqn. (10). It must be noted that the tangential acceleration component is not symmetrical implying that the direction of rotation will potentially have an effect on the LHP performance.

Figure 5 shows typical initial transient responses of the LHP without acceleration. In these cases the input evaporator heat rate,  $Q_{in} = 300\text{W}$  and  $600\text{W}$ , were introduced as a step inputs. The inlet condenser cold plate temperatures were maintained at  $T_{cp} = 31^\circ\text{C}$  and  $56^\circ\text{C}$ . Key evaporator and condenser temperatures and their locations are shown as a function of operational time after the step input heat rate was initiated. Prior to applying the evaporator input heat rate the loop heat pipe was preconditioned to a constant cold plate inlet temperature,  $T_{cp}$ . For the experimental run shown in Fig. 5, the evaporator temperature was initially at ambient temperature and the resultant condenser temperature was due to the fixed inlet condenser cold plate temperature,  $T_{cp}$ . Initially, the liquid temperature in the vapor line (between the evaporator outlet, TC08, and condenser inlet, TC09) is at ambient temperature. With the application of a step increase in the evaporator input heat rate, sensible heating occurs followed by a gradual rise in evaporator temperature, TC04, and sudden rise in the evaporator outlet temperature, TC08, as vapor exits the evaporator. Due to the increased pressure at the outlet of the evaporator, the cold liquid in the vapor line is forced into the condenser resulting in a sudden decrease in the condenser inlet temperature, TC09, followed by a sudden rise in condenser inlet temperature as the vapor from the evaporator enters the condenser. As the cold liquid slug enters the condenser followed by the vapor, downstream condenser temperatures, TC10 and TC11, also display a similar dynamic due to the passing cold liquid slug and subsequently increase as the vapor penetrates deeper into the condenser. Comparing Fig. 5a and 5b one can see the effects varying the evaporator input heat rate,  $Q_{in}$ , and inlet cold plate temperature,  $T_{cp}$ . Most noticeable is the delay in the transient response as well as a reduction in the active portion of the condenser with decreasing evaporator input heat rate and colder inlet cold plate temperature.

Considering the typical transient response of this loop heat pipe without acceleration, one can now compare the transient response with and without the induced forces resulting from a steady-periodic acceleration. Table 1 shows the experimental test matrix for the experimental portion of this investigation. Also shown in Table 1 are informational comments during the course of the experimental runs. For these experiments, the evaporator input heat rate was applied as a step increase either before, mode I operation, or after initiation of the steady-periodic acceleration, mode II operation. The radial acceleration,  $a_r$ , was controlled as a sine wave function with a frequency,  $f = 0.1\text{Hz}, 0.05\text{Hz}, 0.01\text{Hz}$ , and peak-to-peak radial acceleration,  $0.5g \leq a_r \leq 10.0g$ . Once the steady-periodic acceleration was initiated, the input heat rate was varied as a step increase from 0W and experimentally maintained to within  $\pm 5\%$ .

Initially the loop heat pipe was operated to determine the time evolution of both the evaporator and condenser temperatures for a fixed evaporator input heat rate,  $Q_{in} = 300\text{W}$ , and inlet cold plate coolant temperature,  $T_{cp} = 30\text{--}35^\circ\text{C}$ , when subjected to a steady periodic acceleration,  $f = 0.05\text{Hz}$  and  $1.0g \leq a_r \leq 6.0g$ . Figures 6-11 show the time variant temperatures, in five minute increments, across the titanium-water LHP. The temperature measurements shown; consist of evaporator and condenser temperatures, evaporator outlet and condenser inlet temperatures, compensation chamber inlet (TC19 Bayonet In) and outlet (TC20 Evap CC) temperatures. Figure 6 shows the 0-5 minute loop heat pipe temperature response from an initial temperature condition. The transient response to a step input of evaporator heat rate can be compared qualitatively to Fig. 5a, for the case without acceleration. For this case there is a similar transient response with the exception of an additional superimposed oscillatory temperature variation due to the steady-periodic acceleration profile.

Figures 7-11 show various transient operating dynamics in the first 5-40 minutes of operation in five minute increments. Comparison of these dynamics clearly demonstrates the extent to which the motion of the fluid within the loop heat pipe drives the loop heat pipe performance. Specifically, the steady-periodic acceleration oscillation was shown to drive liquid oscillation within the condenser helping to improve performance over the performance with steady-state 6-g acceleration as shown by Fleming et al.<sup>10</sup>. Over time, a variety of dynamics evolve from steady-periodic non-sine wave dynamics to dynamics that are consistent in frequency of the acceleration sine-wave but with the potential for phase shift. As an example, the initial evolution of the steady-periodic dynamics of the compensation chamber temperature, TC20, occurs within 5-25 minutes is shown in Figs 7-9. These dynamics are periodic but with a dynamical form that evolves over time. After 30 minutes, Figs 10-11, the compensation chamber

temperature has evolved to a steady-periodic dynamic at the same frequency, but with a slight phase shift, to the steady-periodic acceleration sine-wave.

The loop heat pipe was then operated to determine the heat transport performance due to the coupling of inputs; evaporator input heat rate,  $Q_{in}$ , inlet condenser cold plate temperature,  $T_{cp}$ , acceleration frequency,  $f$ , and radial acceleration,  $a_r$ , peak-to-peak values. After the aforementioned preconditioning period, the loop heat pipe was operated in two modes. The first mode (Mode I) consisted of initially operating the loop heat pipe to a step increase of the evaporator input heat rate but without acceleration. After approximately one hour of operation, the steady-periodic acceleration was applied to the loop heat pipe. The second mode of operation (Mode II) consisted applying the steady-periodic acceleration prior to the adding the evaporator input heat rate. After several minutes, a step increase in the evaporator input heat rate was applied to the loop heat pipe.

Figures 12 and 13 show the mode I transient loop heat pipe response with and without acceleration, the inlet cold plate temperature,  $T_{cp} = 31^{\circ}\text{C}$  to  $56^{\circ}\text{C}$ , and for an evaporator input heat rate,  $Q_{in} = 600\text{W}$  and  $300\text{W}$ , respectively. Figures 12a and 12c show the transient response to a step increase in the evaporator input heat rate without acceleration. Figures 12b and 12d show the transient response, from steady-state conditions for  $Q_{in} = 600\text{W}$ , to a steady-periodic radial acceleration sine wave with frequency,  $f = 0.01\text{Hz}$ , and peak-to-peak radial acceleration,  $0.5g \leq a_r \leq 10g$ . For both cases the condenser shutdown after applying the steady-periodic acceleration. This can be seen by the sudden decrease in condenser temperature, TC11, indicating condenser shutdown. This resulted in a rapid increase in evaporator temperature, TC4, and subsequent failure of the loop heat pipe. For the case of the inlet cold plate temperature,  $T_{cp} = 31^{\circ}\text{C}$ , shutdown of the condenser occurred within the first cycle of the acceleration transient, Fig. 12b. However, with the inlet cold plate temperature,  $T_{cp} = 56^{\circ}\text{C}$ , shutdown of the condenser occurred during the sixth cycle of the acceleration transient; approximately eight minutes later than that for  $T_{cp} = 31^{\circ}\text{C}$ .

Similar to Fig. 12, Figs. 13a and 13c show the transient response to a step increase in the evaporator input heat rate without acceleration for  $Q_{in} = 300\text{W}$ . Figures 13b and 13d show the transient response, from steady-state conditions for  $Q_{in} = 300\text{W}$ , to a steady-periodic radial acceleration, sine wave, with frequency,  $f = 0.01\text{Hz}$ , and peak-to-peak radial acceleration,  $0.5g \leq a_r \leq 10g$ . For both cases the LHP operated as expected without acceleration. As shown in Fig. 13b, the addition of the acceleration profile resulted in a slight increase in the LHP operating temperature. The condenser temperature located at TC10 oscillated with the same frequency as the acceleration

profile. This also indicated that the liquid-vapor transition point was located and oscillated around the mounting position of TC11. However, as shown in Fig. 13d, with the inlet cold plate temperature,  $T_{cp} = 53^{\circ}\text{C}$ , the LHP failed to run for a sustained period of time. This was evidenced by condenser shutdown approximately at the 20-minute operating point after initiating the acceleration profile.

Figures 14 and 15 show the mode II transient LHP response in a steady-periodic acceleration environment for a step increase in the evaporator input heat rate,  $Q_{in} = 600\text{W}$  and  $300\text{W}$ , respectively. The steady-periodic acceleration was generated as a sine wave for the radial acceleration with frequency,  $f = 0.01\text{Hz}$ , and peak-to-peak radial acceleration,  $0.5g \leq a_r \leq 10g$ . Figures 14a and 14c show the evaporator input heat rate started at the maximum acceleration and  $T_{cp} = 31^{\circ}\text{C}$  and  $51^{\circ}\text{C}$  respectively. Figures 14b and 14d show the evaporator input heat rate started at the minimum acceleration and  $T_{cp} = 31^{\circ}\text{C}$  and  $51^{\circ}\text{C}$  respectively. For the cases shown in Figs. 14a and 14b, with  $T_{cp} = 31^{\circ}\text{C}$ , the LHP failed regardless of whether the evaporator input heat rate was started at the maximum or minimum of the acceleration profile. When the evaporator input heat rate was started at the minimum of the acceleration profile, rather than the maximum, the condenser temperature dynamic response appeared to be somewhat delayed. This is noted by the dynamical temperature response of TC09 and TC10. The exception to this is the condenser temperature reflected by TC11. At this location in the condenser there was an increase in temperature followed by a temperature decrease that was a precursor to the condenser shutting down with a subsequent failure in the LHP operation. For the case of the evaporator heat rate initiated at the maximum of the acceleration profile there was a significant delay in the condenser temperature dynamic response, at the TC11 location, compared to the case of the evaporator heat rate initiated at the minimum of the acceleration profile.

However for  $T_{cp} = 51^{\circ}\text{C}$ , Figs. 14c and 14d, the LHP operated in a normal fashion with some differences in the startup dynamics. Of particular note are the variations in dynamical temperature responses of condenser temperatures TC09, TC10, and TC11 resulting from the evaporator input heat rate started either at the maximum or minimum of the acceleration profile. These variations in the dynamical temperature responses consisted of the narrowing of or broadening of the temperature spike due to the cold liquid slug passing through the condenser. The dynamical temperature profile of TC11 also showed a significant delay in the temperature rise once the liquid slug had passed the condenser location of TC11. This may be due to acceleration induced forces impeding the liquid-vapor flow required to open up the condenser sufficiently to sustain normal operation.



Similar to Fig. 14, Fig. 15 shows the evaporator input heat rate,  $Q_{in} = 300W$ , initiated at either the acceleration minimum or maximum. Figs. 15a and 15c show the LHP initial temperature response when started at the maximum acceleration with  $T_{cp} = 30^{\circ}C$  and  $52^{\circ}C$  respectively. Figures 15b and 15d show the LHP initial temperature response when started at the minimum acceleration with  $T_{cp} = 30^{\circ}C$  and  $50^{\circ}C$  respectively. As shown in Figs. 15a and 15b, it was generally noted that there very little deviation in the transient of the LHP response for the inlet cold plate temperature,  $T_{cp} = 30^{\circ}C$ . However for  $T_{cp} = 50^{\circ}C$  and  $52^{\circ}C$ , Figs. 15c and 15d, there was a notable change in the LHP dynamics which led, in both cases, to a slow degradation to failure or “graceful failure.” The differences in the dynamics can be seen in both a delay and widening of the temperature spikes as the cold liquid slug is forced through the condenser.

Figure 16 shows the results for an increase in the frequency,  $f$ , of the acceleration profile. Figs. 16a and 16c show the transient LHP response without acceleration for a step increase in the evaporator input heat rate,  $Q_{in} = 600W$ , and input cold plate temperature,  $T_{cp} = 30^{\circ}C$  and  $50^{\circ}C$ , respectively. Figures 16b and 16d show the transient LHP response for the steady-periodic radial acceleration frequencies,  $f = 0.05Hz$  and  $0.1Hz$ , respectively. Figure 16b shows this transient response for the peak-to-peak radial acceleration,  $0.5g \leq a_r \leq 6g$ , and  $T_{cp} = 32^{\circ}C$  while Fig. 16d shows the transient response for the peak-to-peak radial acceleration,  $0.5g \leq a_r \leq 10g$ , and  $T_{cp} = 52^{\circ}C$ . For both cases, there were only slight variations in the LHP transient response with and without acceleration. The steady-periodic acceleration imposed an oscillatory temperature, as evidenced by the transient thermocouple response, most likely due to the periodic fluid motion within the LHP. However, the acceleration frequency in these cases did not appear to otherwise significantly alter the LHP performance.

Figures 17-20 show the transient LHP response due to varying the minimum radial acceleration,  $a_{r_{min}}$ , for a steady-periodic acceleration with frequency,  $f = 0.055Hz$ , with a maximum peak acceleration,  $a_{r_{max}} = 7g$ . The evaporator input heat rate was applied as step increase,  $Q_{in} = 450W$ , with a cold plate inlet temperature,  $T_{cp} = 42^{\circ}C$ . Figure 17 shows the extended transient response for  $a_{r_{min}} = 0.5g$ ,  $1.0g$ , and  $1.5g$ . Figure 18 shows the initial transient response with varying  $a_{r_{min}}$ . Figures 19 and 20 show the acceleration driven transitory responses leading to either a transitory partial condenser shutdown or permanent partial condenser shutdown. Figures 17-20 also expand the temperature information to include the condenser outlet temperature, TC17, and compensation chamber inlet and outlet temperatures, TC19 and TC20 respectively. Also shown is the compensation chamber wall temperature, TC21. The compensation chamber wall temperature shown in the plots is one of several thermocouples mounted

around the centerline circumference of the compensation chamber. During the experiments temperature differences around the circumference of compensation chamber were within the thermocouple calibration uncertainty. It must also be noted that due to the linear construction of both the condenser/cold plate and evaporator/compensation chamber, the evaporator/compensation chamber is also subjected to a similar acceleration gradient as the condenser, Fig. 3.

Varying the minimum radial acceleration,  $ar_{min}$ , resulted in significant variations in the long-term LHP performance, Fig. 17. As shown in Fig. 18, the initial dynamical response showed little change when  $ar_{min}$  was varied. However, after 20-30 minutes the LHP exhibited a unique temperature response, Figs. 17a and 17b, driven by either a transitory partial or permanent partial change in condenser performance with the liquid-vapor front moving toward the evaporator. For the case where  $ar_{min} = 1.5g$ , Fig. 17a, the evaporator temperature increased toward a dry out event but ultimately recovered to a stable operating condition although at an elevated temperature consistent with a permanent partial condenser shutdown. For  $ar_{min} = 1.0g$ , Fig. 17b, there were multiple evaporator temperature spikes possibly due to the transitory condenser operation. For this case the LHP also operated at a stable operating condition, although at an elevated evaporator temperature. For  $ar_{min} = 0.5g$ , the LHP operated in a stable manner consistent with a typical LHP steady-state response. For all three cases, the compensation chamber wall temperature remained constant for approximately 70 minutes after which there was a gradual increase in wall temperature until the LHP was experimentally shutdown.

Figures 19 and 20 show the detailed temperature response during the partial condenser shutdown events while varying the minimum acceleration,  $ar_{min}$ . From these plots there is not a clear role for that of the compensation chamber inlet or outlet temperatures as a dynamic contributor to these partial condenser shutdown events. Increased thermocouple placements on the condenser will increase the spatial resolution needed to increase the transitory resolution to determine the time-variant liquid-vapor interface location. This will help to determine the time variant sequence of events driving the LHP dynamical performance.

In general, if one considers the testing of this LHP to a steady-state radial acceleration by Fleming et al.<sup>10</sup>, there appears to be a correlation with the maximum steady-state radial acceleration and the peak radial acceleration,  $ar_{max}$ . If the peak radial acceleration,  $ar_{max}$ , is equal to or greater than the maximum steady-state radial acceleration, there is a greater likelihood that the LHP will fail. This is particularly true if the minimum radial acceleration,  $ar_{min}$ , is increased. Figure 21 shows the steady-state performance plotted with the heat transported by Fleming et al.<sup>10</sup> For

this current study, the heat rate transported is on the order of 70% of the evaporator input heat rate,  $Q_{in}$ , resulting is a transported heat rate of approximately 315W. From Fig. 21 the maximum steady-state radial acceleration for this case is between 4g-6g which is less than the peak radial acceleration,  $ar_{max} = 7g$ . As such, there should be an expectation that the LHP will fail as the minimum radial acceleration,  $ar_{min}$ , is increased. For the cases shown in Fig. 17 there were also distinct regions of LHP operation with degraded performance as the minimum radial acceleration,  $ar_{min}$ , was increased. It may also be possible to correlate the maximum steady-state acceleration value to the maximum peak-to-peak steady-periodic acceleration using either the root mean square (RMS) or average values of the acceleration transient.

## V. Conclusions

Dynamic forces generated from acceleration transients, when combined with thermodynamic forces, can significantly impact the dynamical performance of a LHP. In some cases acceleration driven forces can compliment thermodynamic forces improving LHP dynamical performance. However, the converse is also true in that transient acceleration driven forces can also counter thermodynamic forces. This can result in immediate total failure of the LHP to operate, delayed total failure, or in some cases, in stable operation but in a degraded condition. Either way, one should clearly understand the nature of the resulting forces, i.e. magnitude and direction, which are generated from a transitory and spatial acceleration vector field and their impact on the dynamical performance of two-phase thermodynamic systems such as LHPs.

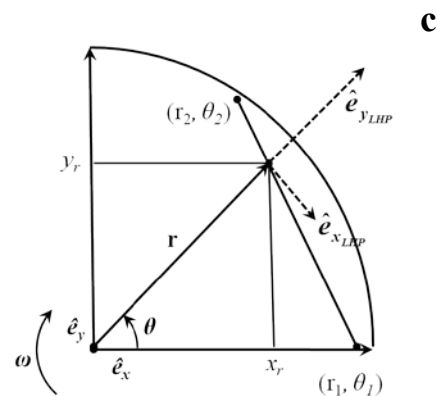
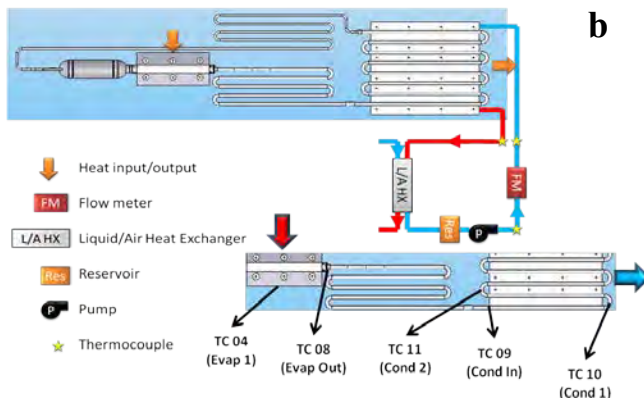
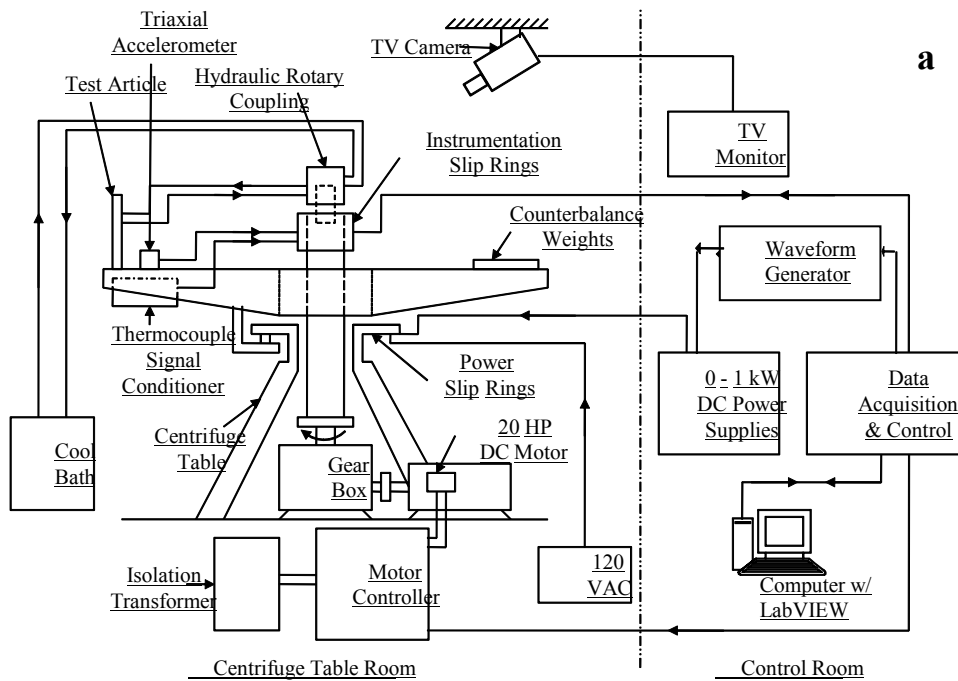
Transient acceleration frequency and peak-to-peak amplitude combined with the LHP operating history appear to be a critical factor in the performance of the LHP. Whether the LHP is operating prior to or started up after an acceleration transient can result in differing LHP dynamical performance characteristics. In general, it appears that the higher the acceleration frequency and peak-to-peak amplitude the less detrimental influence there is on the LHP performance. For these cases, there appears to be an improved LHP performance due to the increased motion of condensate within the LHP condenser driven by the acceleration component along the length of the LHP. Conversely, decreased acceleration frequency and increased peak-to-peak amplitude appear to have a greater detrimental influence on the LHP performance. This is particularly true if the magnitude of the acceleration peak is near to or exceeds a failure mode for the LHP subjected to steady-state acceleration. Furthermore, as the frequency is decreased the resulting LHP performance should be consistent with and approaching that of a LHP subjected to

steady-state acceleration. There also appeared to be natural oscillation of the fluid in the condenser during the LHP operation when subjected to steady-state acceleration in frequencies ranging from 0.008Hz to 0.2Hz. Exciting these natural frequencies through a transient acceleration may also lead to failure of the LHP to operate.

Conclusions drawn from past LHP performance studies, with steady-state acceleration, should also be considered as special cases. One should be careful not to infer or draw any conclusions toward the dynamical performance behavior or stability of the LHP in transitory acceleration environments from steady-state acceleration testing. However, steady-state testing can provide valuable information regarding the operational limits of a LHP provided one understands the nature of the forces generated from either a steady-state or transitory acceleration field.


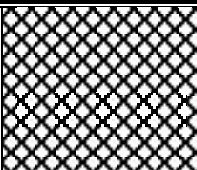
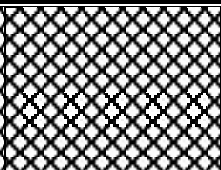
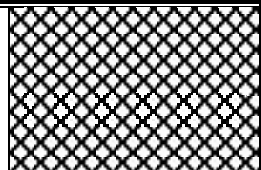
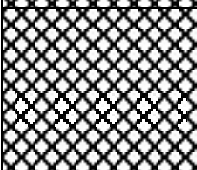
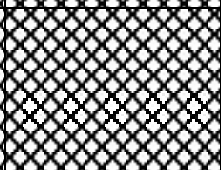
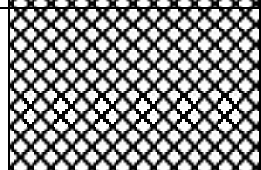
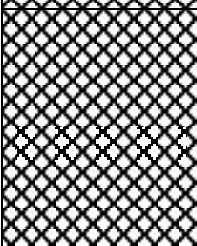
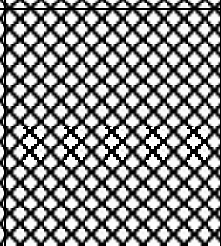
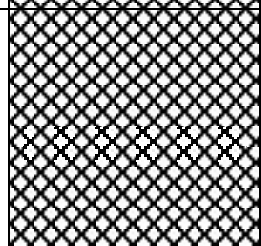
## VI. References

- [1] Ku, J., "Operating characteristics of Loop Heat Pipes," 29<sup>th</sup> International Conference on Environmental Systems, July 12-15, 1999.
- [2] Ku, J., Ottenstein, L., Kobel, M., Rogers, P., Kaya, T., "Temperature Oscillations in Loop Heat Pipe Operation," Space Technology and Applications International Forum, 2001.
- [3] Bai, L., Lin, G., Zhang, H., Wen, D., "Mathematical Modeling of Steady-State Operation of a Loop Heat Pipe," *Applied Thermal Engineering*, Vol. 29, 2009, pp. 2643-2654.
- [4] Bai, L., Lin, G., Wen, D., "Modeling and Analysis of Startup of a Loop Heat Pipe," *Applied Thermal Engineering*, Vol. 30, 2010, pp.2778-2787.
- [5] Shukla, K., "Thermo-fluid dynamics of Loop Heat Pipe Operation," *International Communications in Heat and Mass Transfer*, Vol. 35, 2008, pp. 916-920.
- [6] Khrustalev, D., "Advances in Transient Modeling of Loop Heat Pipe Systems with Multiple Components," Space, Propulsion and Energy Sciences International Forum, 2010.
- [7] Hoang, T., "Stability and Oscillations in Loop Heat Pipe Operations: A Classic Non-Linear Dynamics Problem," International Two-Phase Thermal Control Workshop, University of Maryland, 31October 2011-3November 2011.
- [8] Ku, J., Ottenstein, L., Kaya, T., Rogers, P., and Hoff, C., "Testing of a Loop Heat Pipe Subjected to Variable Accelerating Forces, Part1: Start-Up," SAE Paper 2000-0102488, July 2000.
- [9] Ku, J., Ottenstein, L., Kaya, T., Rogers, P., and Hoff, C., "Testing of a Loop Heat Pipe Subjected to Variable Accelerating Forces, Part2: Temperature Stability," SAE Paper 2000-0102489, July 2000.
- [10] Fleming, A., Thomas, S.K., Yerkes, K., "Titanium-Water Loop Heat Pipe Operating Characteristics Under Standard and Elevated Acceleration Fields," *Journal of Thermophysics and Heat Transfer*, Vol. 24, 2010, pp.184-198. DOI: 10.2514/45684



**Figure 1. Experimental schematics showing the (a) centrifuge, (b) titanium-water loop heat pipe experimental setup, and (c) centrifuge and accelerometer coordinate system corresponding to the condenser mounting location.**

**Table 1. Experimental test matrix**

			Mode I operation (Start heat before acceleration)		Mode II operation (Start acceleration before heat)	
f (Hz)/ar pk-pk (g)	Tcp (°C)	Qin (W)	before accel	adding accel	heat added at max ar	heat added at min ar
0.01Hz/0.5-6g	30-35	600	Ran	(Failed) *Failed in 8 min	Ran *Close to failure	Ran *Close to failure
0.01Hz/0.5-10g	30-35		Ran	(Failed) *Failed in 7 min	(Failed) *Failed in 20 min	(Failed) *Failed in 19 min
	50-55		Ran	(Failed) *Failed in 18 min	Ran *Condenser open ~75%	Ran *Condenser open ~75%
0.05Hz/0.5-6g	30-35		Ran	Ran	-----	Ran
0.1Hz/0.5-10g	50-55		Ran	Ran	-----	Ran
0.01Hz/0.5-10g	30-35	300	Ran	Ran	Ran	Ran
	50-55		Ran	Ran *gradually heading toward a “graceful” failure	Ran *gradually heading toward a “graceful” failure	Ran *gradually heading toward a “graceful” failure
0.05Hz/1-6g	30-35		Ran	Ran	-----	Ran
0.055Hz/0.5-7g	40-45	450			Ran *Stable operation no periodic variation	
0.055Hz/1.0-7g	40-45				Ran *Steady-periodic condenser behavior	
0.055Hz/1.5-7g	40-45				Ran *Close to failure; condenser shut down then opened up	

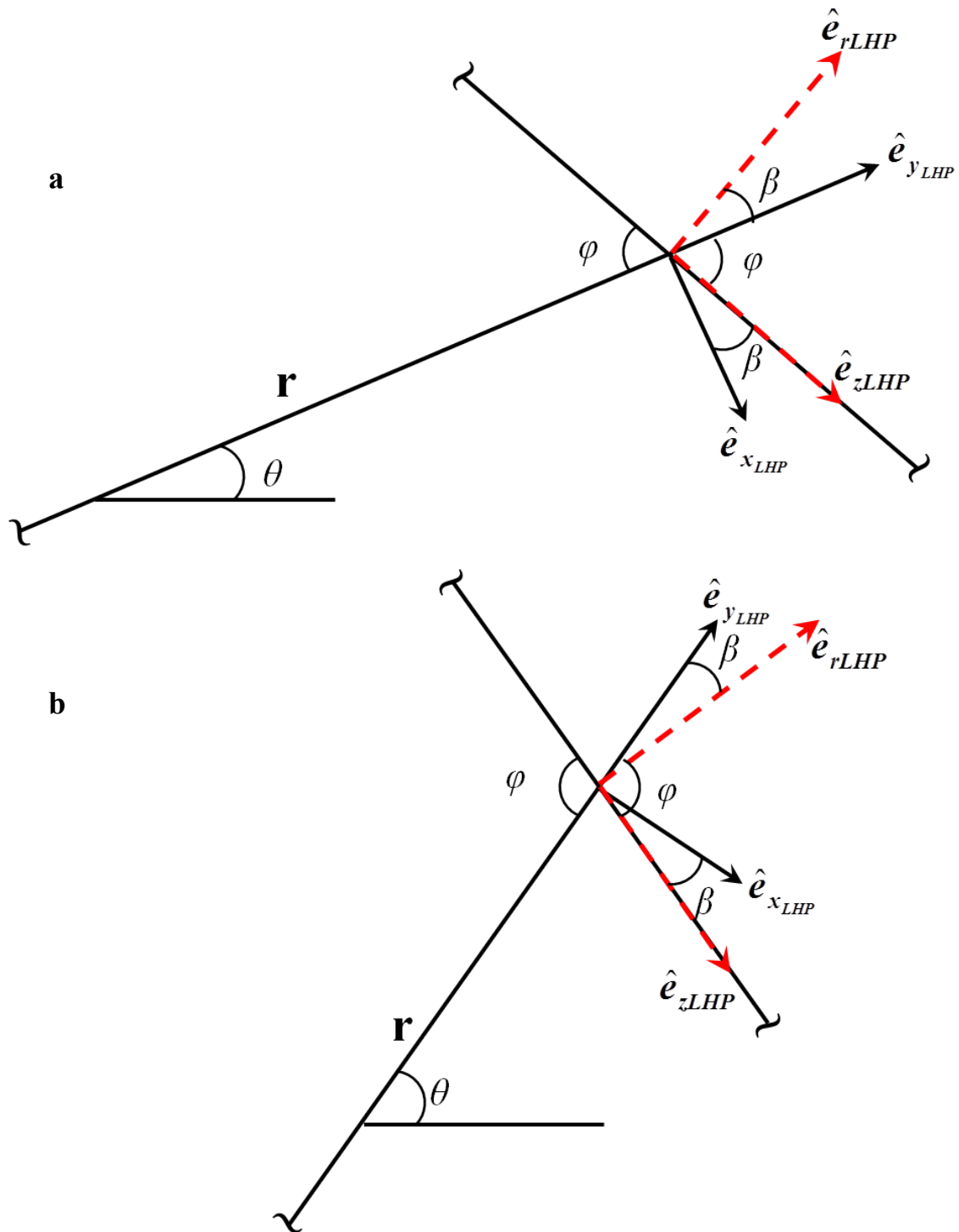
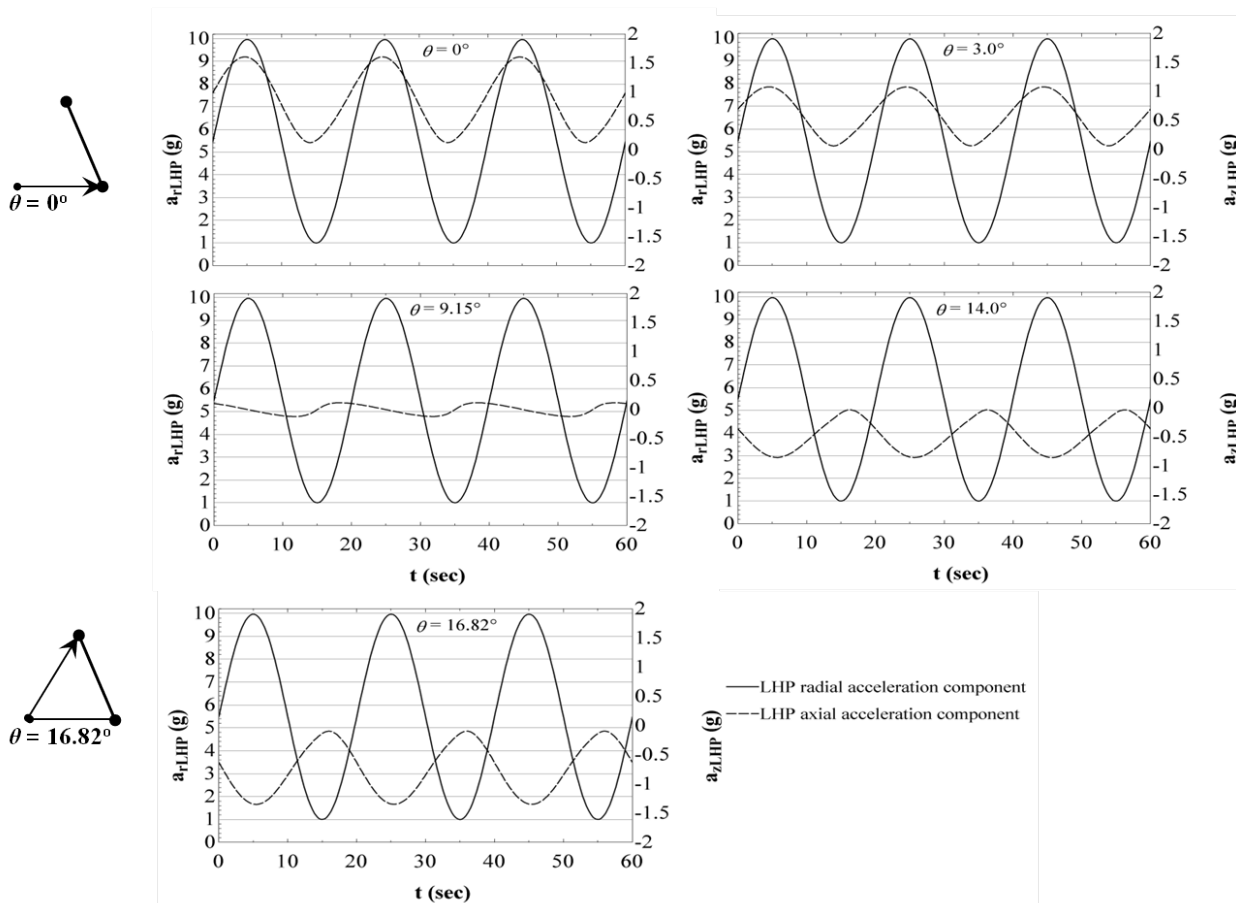


Figure 2. Accelerometer reference frame rotated to align with the LHP radial and axial coordinate system for (a)  $\varphi < 90^\circ$  and  $\beta = (90^\circ - \varphi)$  and (b)  $\varphi > 90^\circ$  and  $\beta = (\varphi - 90^\circ)$ .





**Figure 3.** The radial,  $a_{rLHP}$ , and axial,  $a_{zLHP}$ , acceleration components referenced to the LHP condenser for varying position vector angle,  $\theta$ .

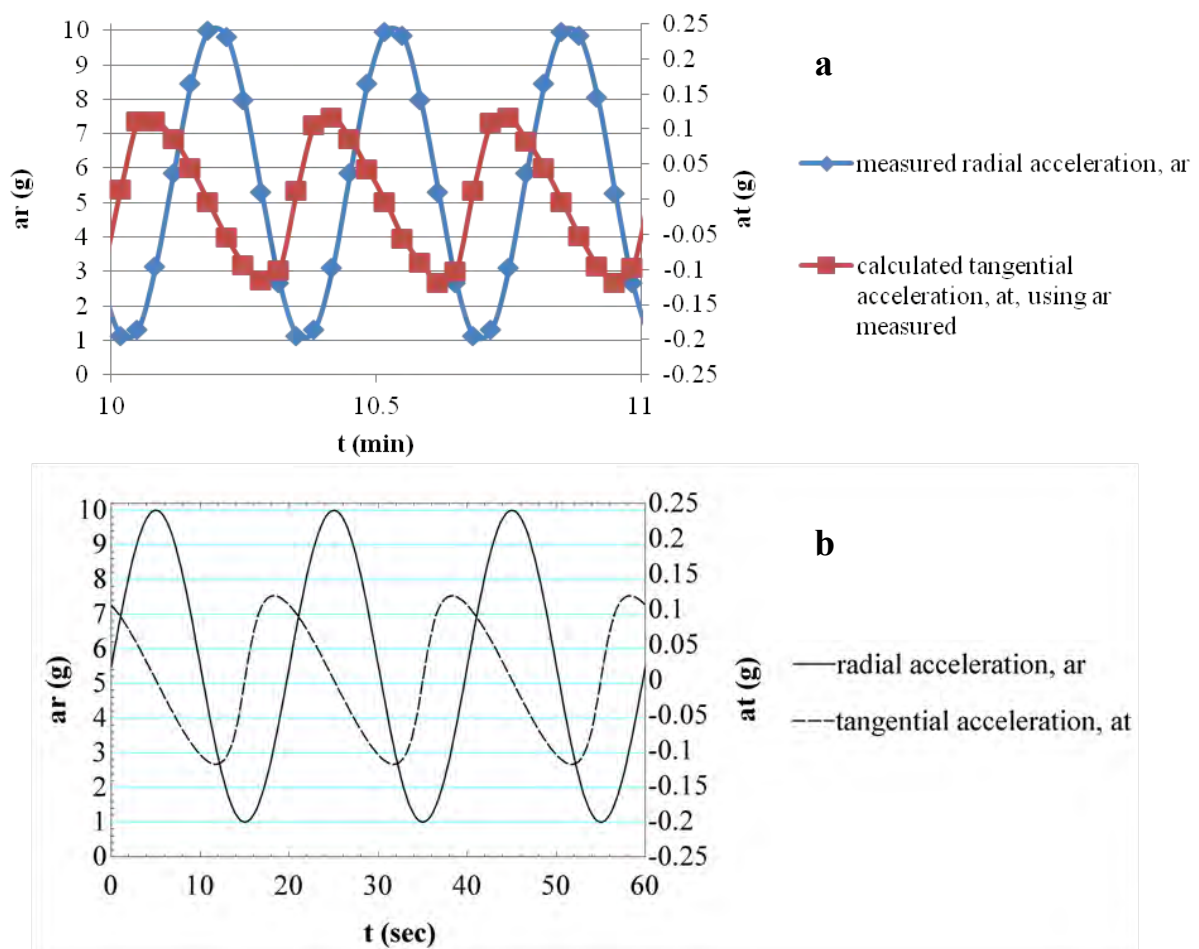


Figure 4. Comparison of experimental to calculated acceleration components, for  $\theta = 14^\circ$ ,  $f = 0.05\text{Hz}$ ,  $1.0g \leq a_r \leq 10.0g$ , where (a) the acceleration is obtained from the experimental accelerometer and (b) the acceleration is calculated using Eqn. (10).

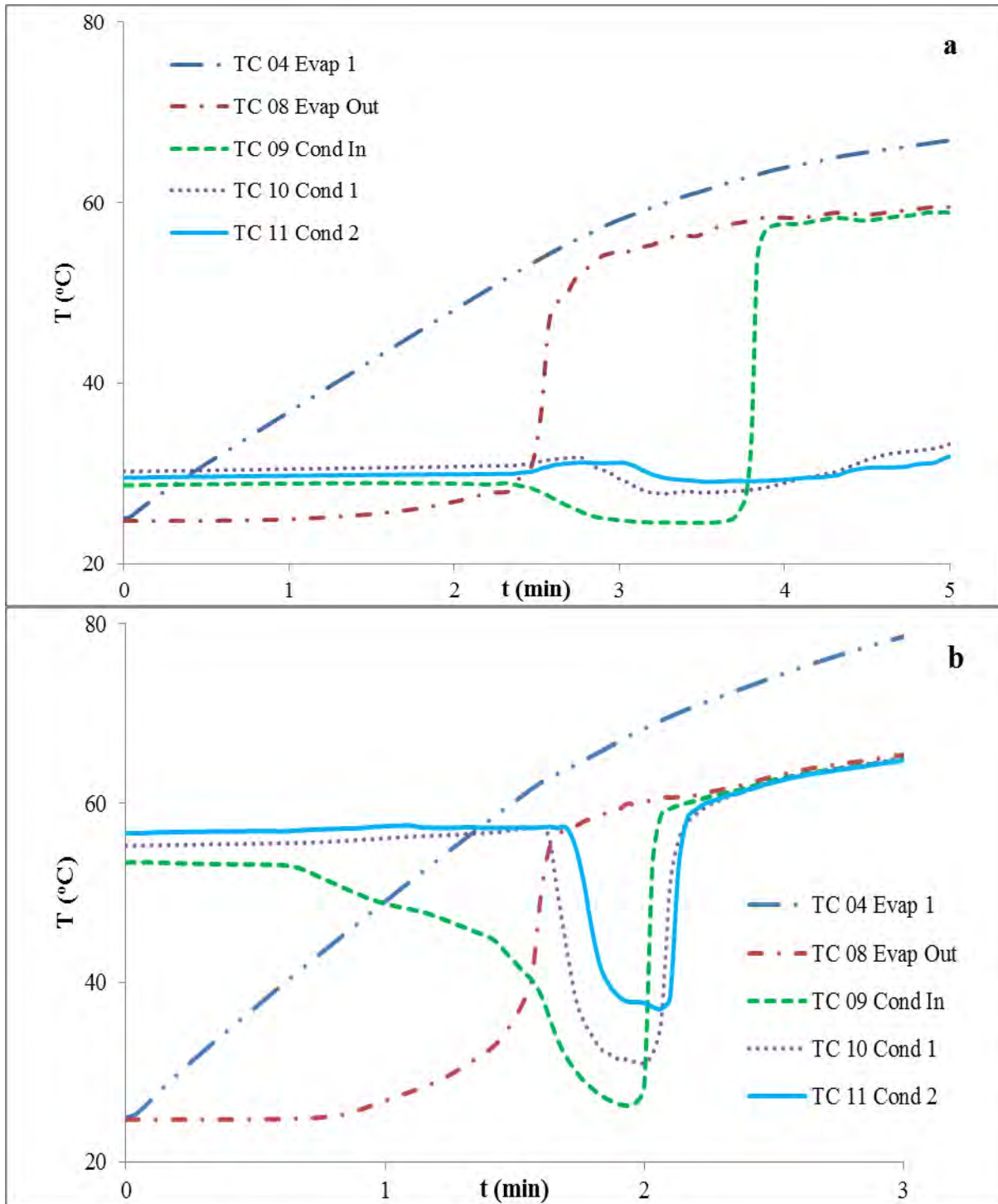


Figure 5. Typical loop heat pipe initial transient response without acceleration and subjected to (a) a step input evaporator heat rate,  $Q_{in} = 300\text{W}$  and inlet condenser cold plate temperature,  $T_{cp} = 31^{\circ}\text{C}$  and (b) a step input evaporator heat rate,  $Q_{in} = 600\text{W}$  and inlet condenser cold plate temperature,  $T_{cp} = 56^{\circ}\text{C}$ .

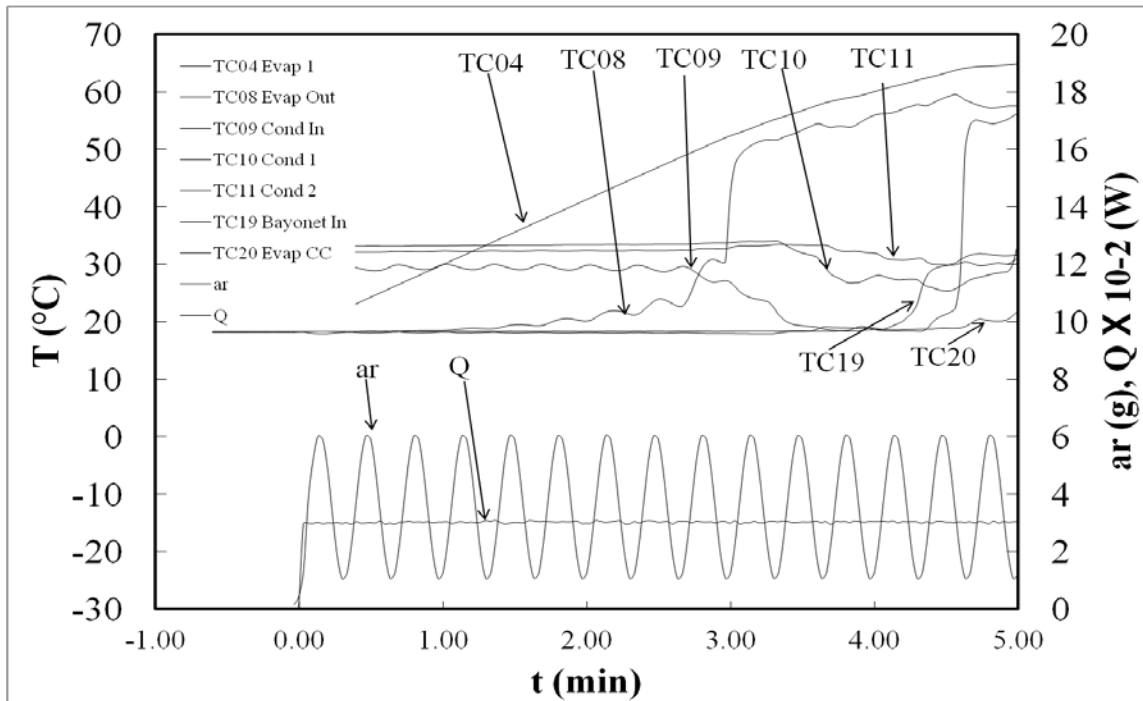


Figure 6. Loop heat pipe initial temperature response for 0-5 minutes. Evaporator input heat rate,  $Q_{in} = 300W$ , inlet cold plate coolant temperature,  $T_{cp} = 30-35^{\circ}C$ , and steady-periodic acceleration,  $f = 0.05Hz$  and  $1.0g \leq ar \leq 6.0g$ .

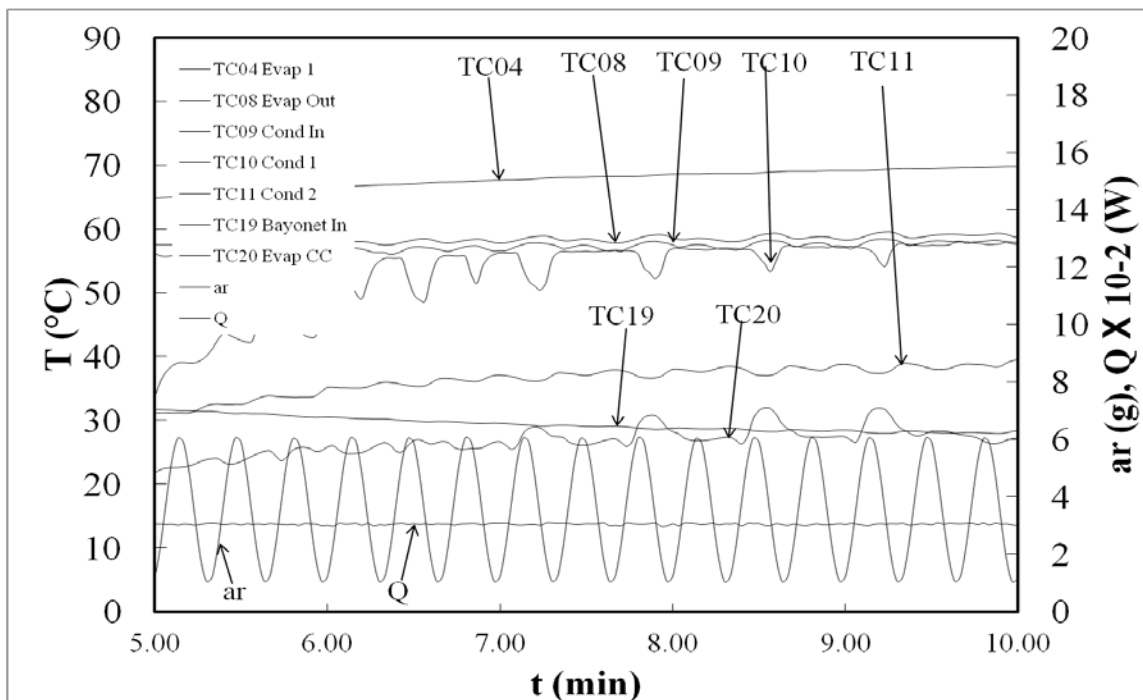


Figure 7. Loop heat pipe temperature response for 5-10 minutes. Evaporator input heat rate,  $Q_{in} = 300W$ , inlet cold plate coolant temperature,  $T_{cp} = 30-35^{\circ}C$ , and steady-periodic acceleration,  $f = 0.05Hz$  and  $1.0g \leq ar \leq 6.0g$ .

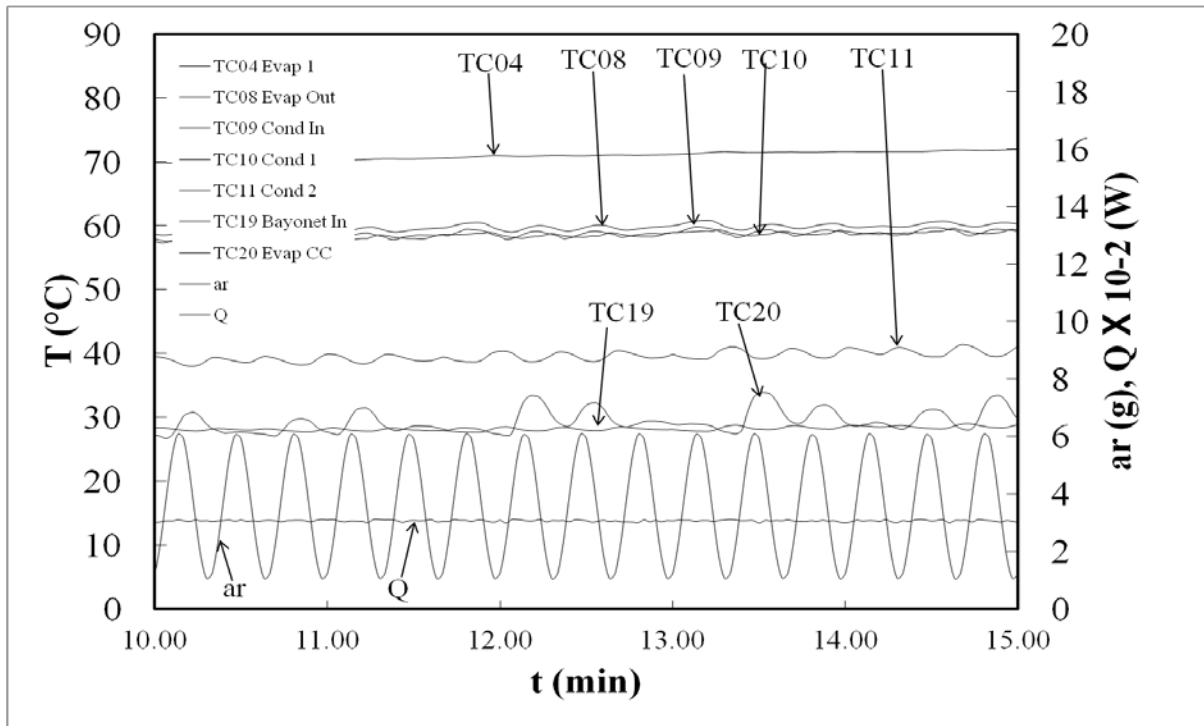


Figure 8. Loop heat pipe temperature response for 10-15 minutes. Evaporator input heat rate,  $Q_{in} = 300W$ , inlet cold plate coolant temperature,  $T_{cp} = 30-35^{\circ}C$ , and steady-periodic acceleration,  $f = 0.05Hz$  and  $1.0g \leq ar \leq 6.0g$ .

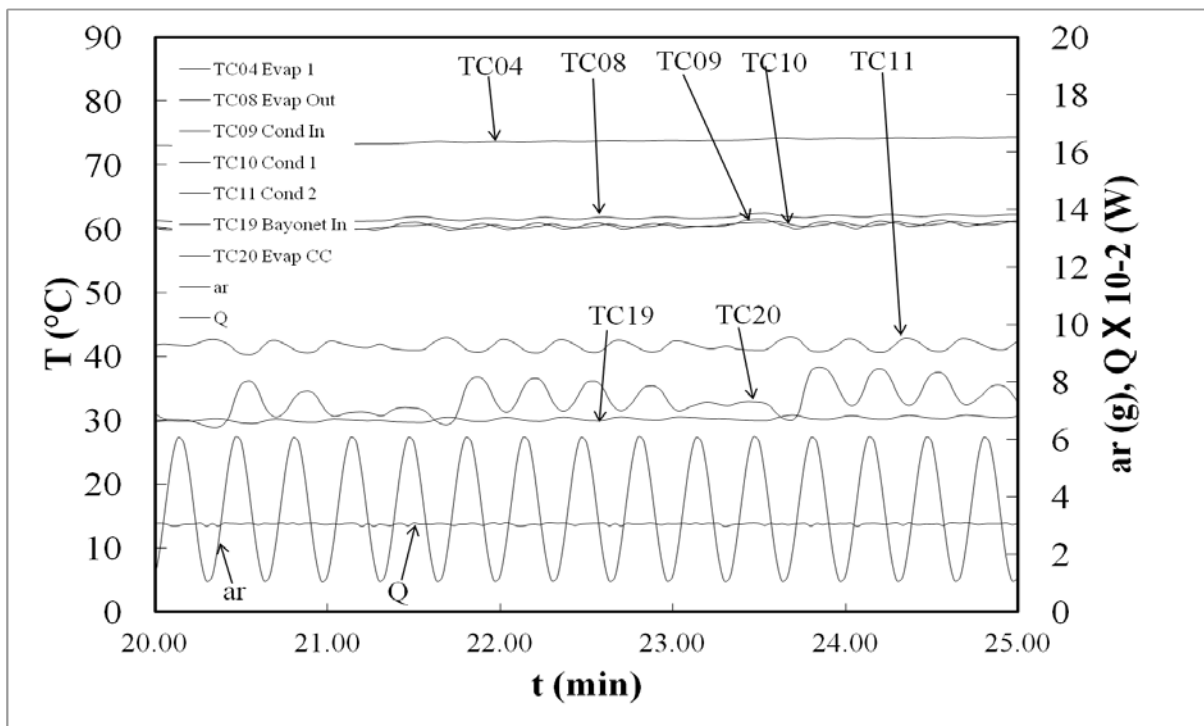


Figure 9. Loop heat pipe temperature response for 20-25 minutes. Evaporator input heat rate,  $Q_{in} = 300W$ , inlet cold plate coolant temperature,  $T_{cp} = 30-35^{\circ}C$ , and steady-periodic acceleration,  $f = 0.05Hz$  and  $1.0g \leq ar \leq 6.0g$ .

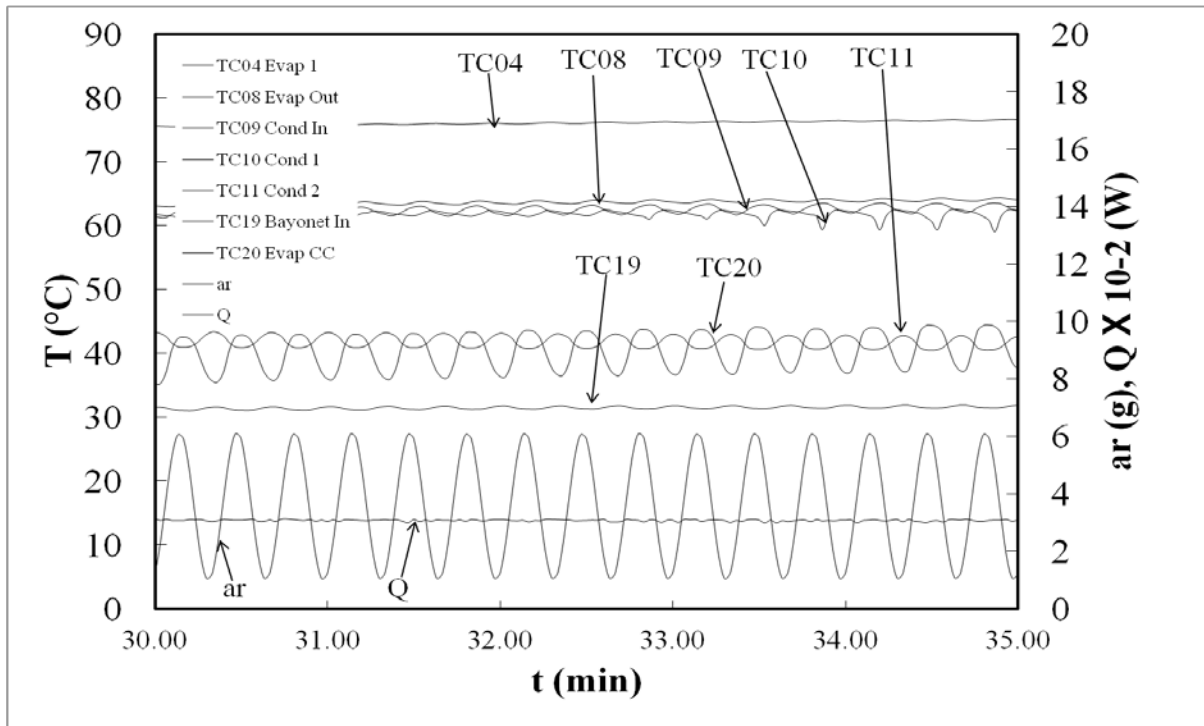


Figure 10. Loop heat pipe temperature response for 30-35 minutes. Evaporator input heat rate,  $Q_{in} = 300\text{W}$ , inlet cold plate coolant temperature,  $T_{cp} = 30\text{-}35^\circ\text{C}$ , and steady-periodic acceleration,  $f = 0.05\text{Hz}$  and  $1.0\text{g} \leq a_r \leq 6.0\text{g}$ .

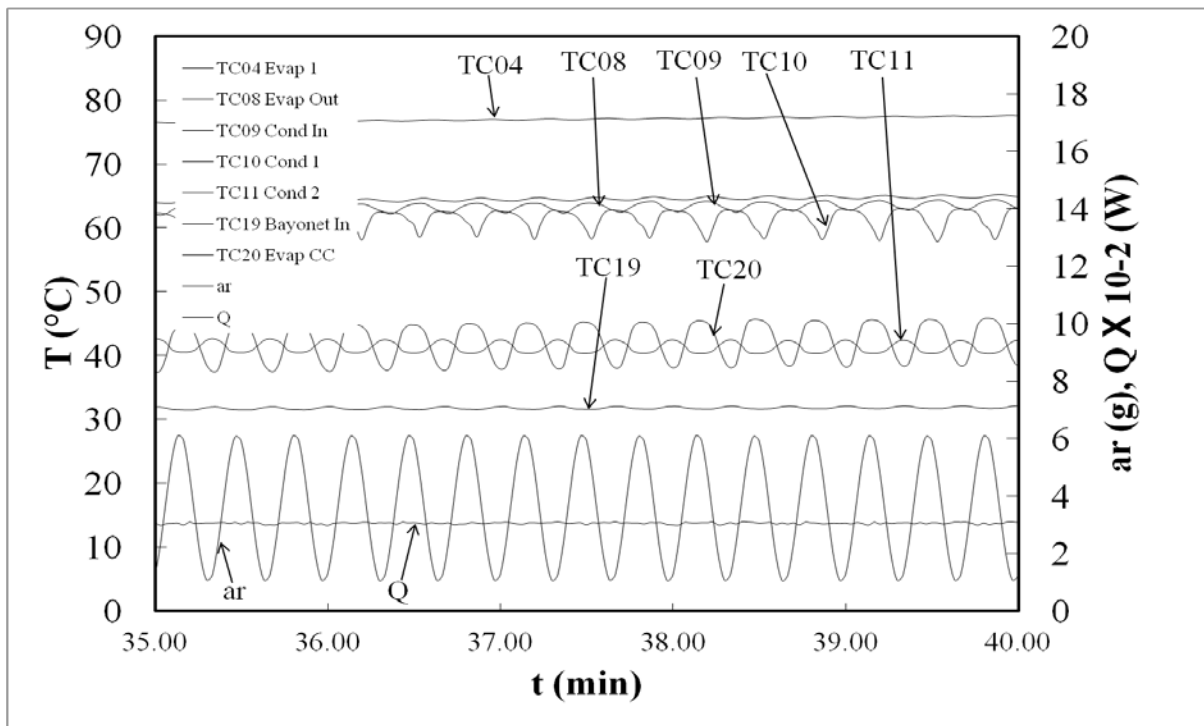


Figure 11. Loop heat pipe temperature response for 35-40 minutes. Evaporator input heat rate,  $Q_{in} = 300\text{W}$ , inlet cold plate coolant temperature,  $T_{cp} = 30\text{-}35^\circ\text{C}$ , and steady-periodic acceleration,  $f = 0.05\text{Hz}$  and  $1.0\text{g} \leq a_r \leq 6.0\text{g}$ .

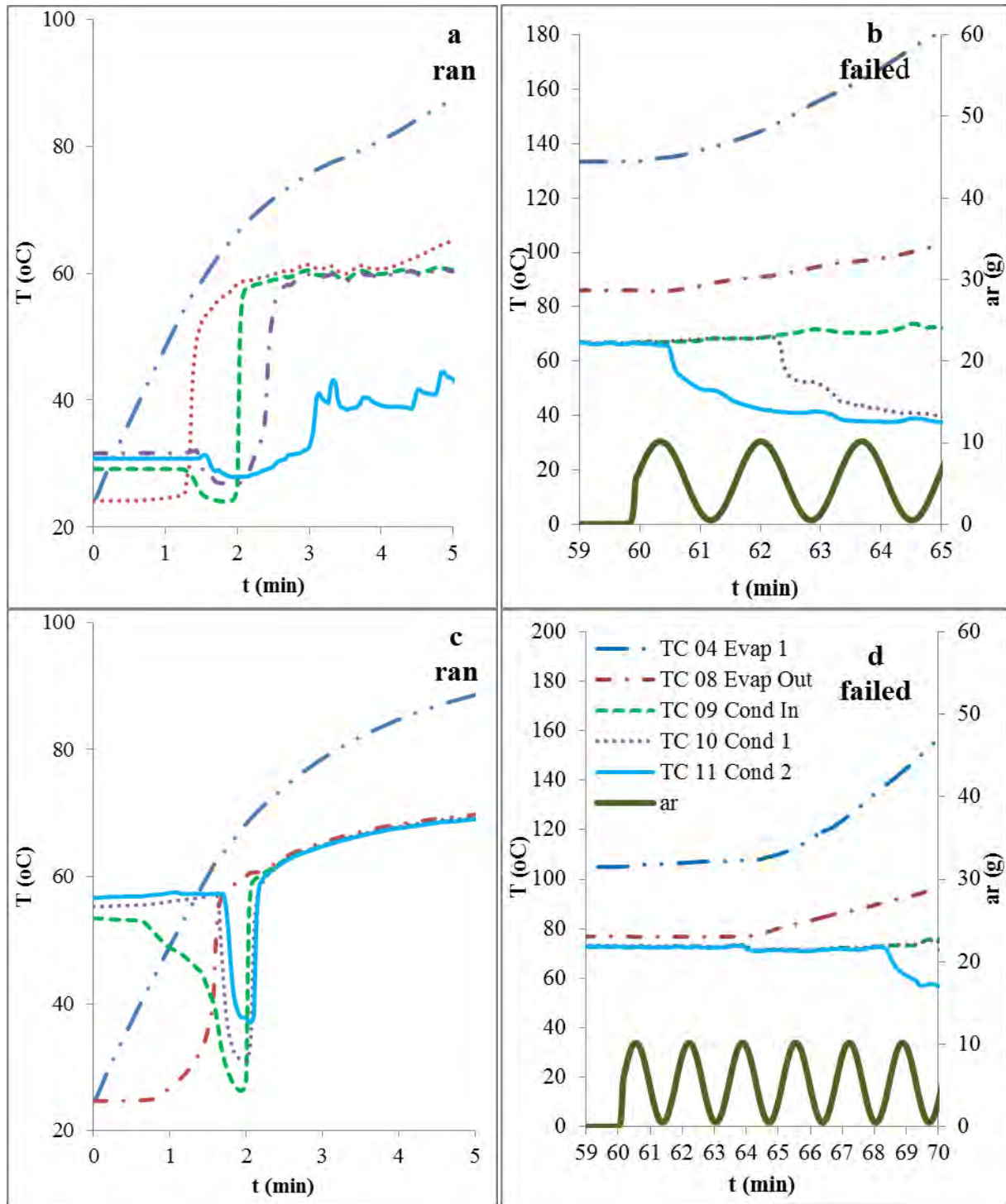


Figure 12. Mode I transient loop heat pipe response to (a) a step input evaporator heat rate,  $Q_{in} = 600\text{W}$ , no acceleration and  $T_{cp} = 31^\circ\text{C}$ , (b) a steady-periodic radial acceleration, sine wave, with frequency,  $f = 0.01\text{Hz}$  with peak-to-peak amplitude,  $0.5g \leq a_r \leq 10g$  at steady-state conditions for  $Q_{in} = 600\text{W}$  and  $T_{cp} = 31^\circ\text{C}$ , (c) a step input evaporator heat rate,  $Q_{in} = 600\text{W}$ , no acceleration and  $T_{cp} = 56^\circ\text{C}$ , and (d) a steady-periodic radial acceleration, sine wave, with frequency,  $f = 0.01\text{Hz}$  with peak-to-peak amplitude,  $0.5g \leq a_r \leq 10g$  at steady-state conditions for  $Q_{in} = 600\text{W}$  and  $T_{cp} = 56^\circ\text{C}$ .



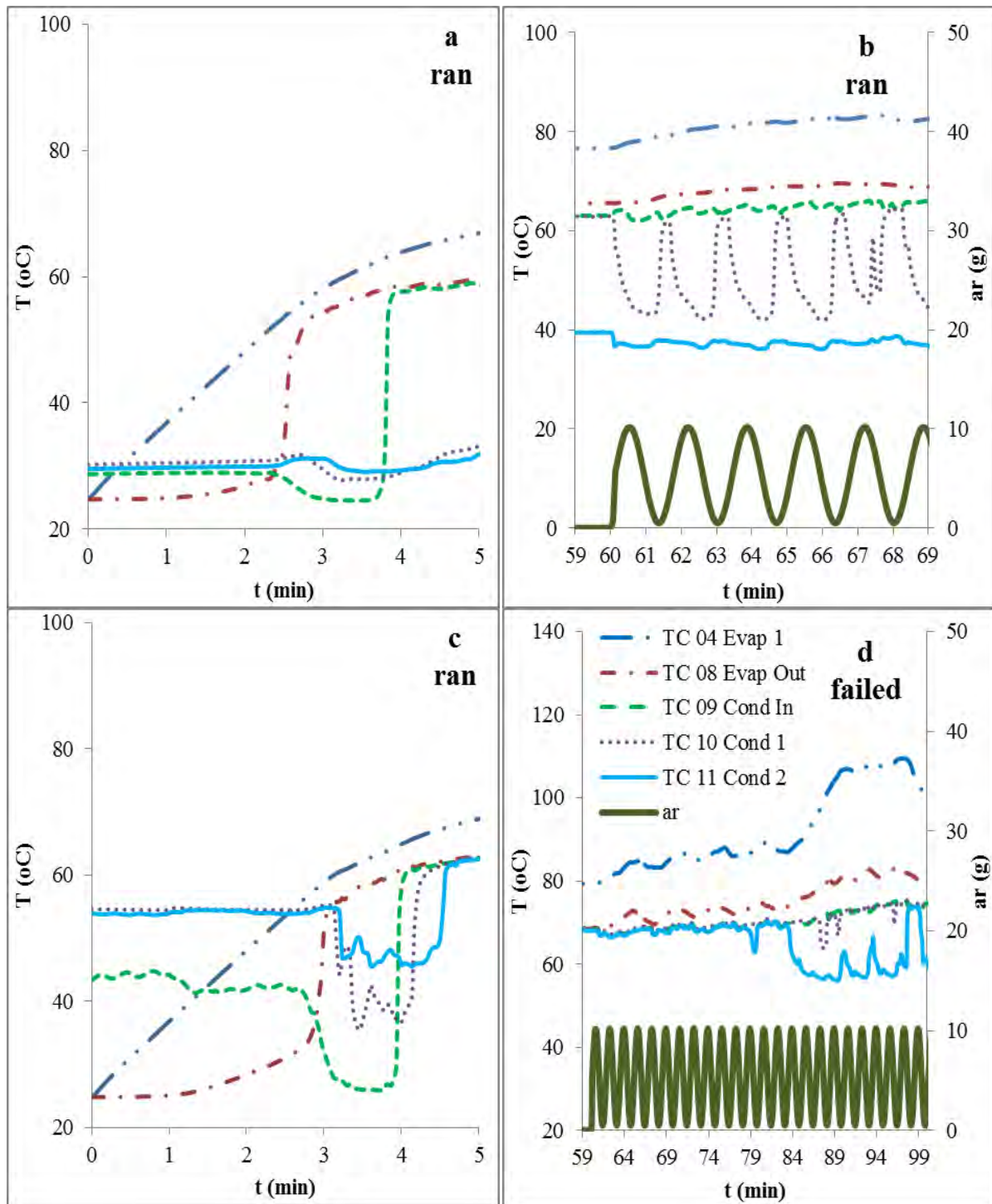


Figure 13. Mode I transient loop heat pipe response for an evaporator heat rate to (a) a step input evaporator heat rate,  $Q_{in} = 300\text{W}$ , no acceleration and  $T_{cp} = 31^\circ\text{C}$ , (b) a steady-periodic radial acceleration, sine wave, with frequency,  $f = 0.01\text{Hz}$  with peak-to-peak amplitude,  $0.5\text{g} \leq ar \leq 10\text{g}$  at steady-state conditions for  $Q_{in} = 300\text{W}$  and  $T_{cp} = 31^\circ\text{C}$ , (c) a step input evaporator heat rate,  $Q_{in} = 300\text{W}$ , no acceleration and  $T_{cp} = 53^\circ\text{C}$ , and (d) a steady-periodic radial acceleration, sine wave, with frequency,  $f = 0.01\text{Hz}$  with peak-to-peak amplitude,  $0.5\text{g} \leq ar \leq 10\text{g}$  at steady-state conditions for  $Q_{in} = 300\text{W}$  and  $T_{cp} = 53^\circ\text{C}$ .



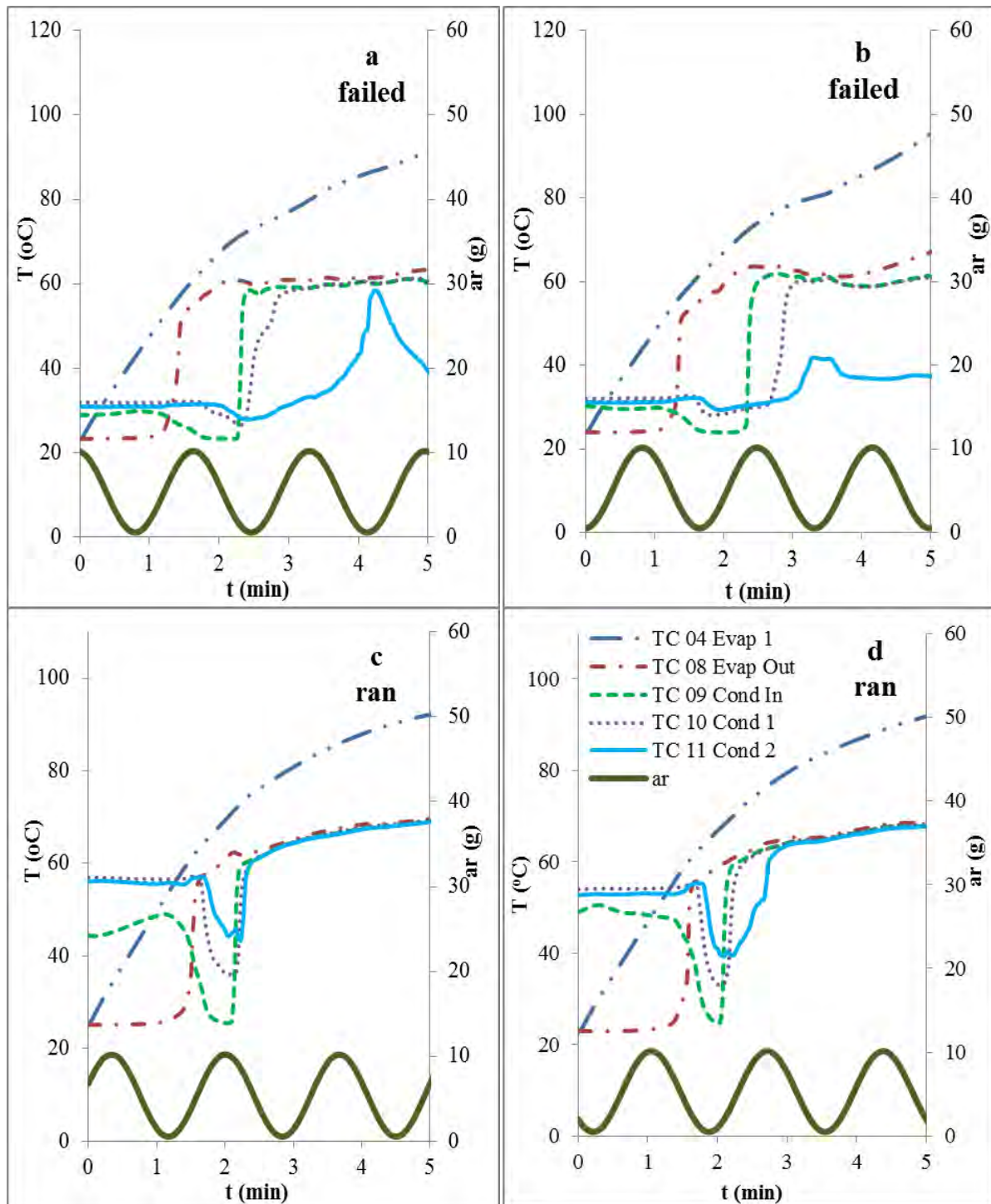


Figure 14. Mode II transient loop heat pipe response for a step input evaporator heat rate,  $Q_{in} = 600\text{W}$ , with a steady-periodic radial acceleration, in the form of a sine wave, with frequency,  $f = 0.01\text{Hz}$ , and peak-to-peak amplitude,  $0.5\text{g} \leq a_r \leq 10\text{g}$ , for (a) the heat input started at max acceleration and  $T_{cp} = 31^{\circ}\text{C}$ , (b) the heat input started at min acceleration and  $T_{cp} = 31^{\circ}\text{C}$ , (c) the heat input started at max acceleration and  $T_{cp} = 51^{\circ}\text{C}$ , and (d) the heat input started at min acceleration and  $T_{cp} = 51^{\circ}\text{C}$ .

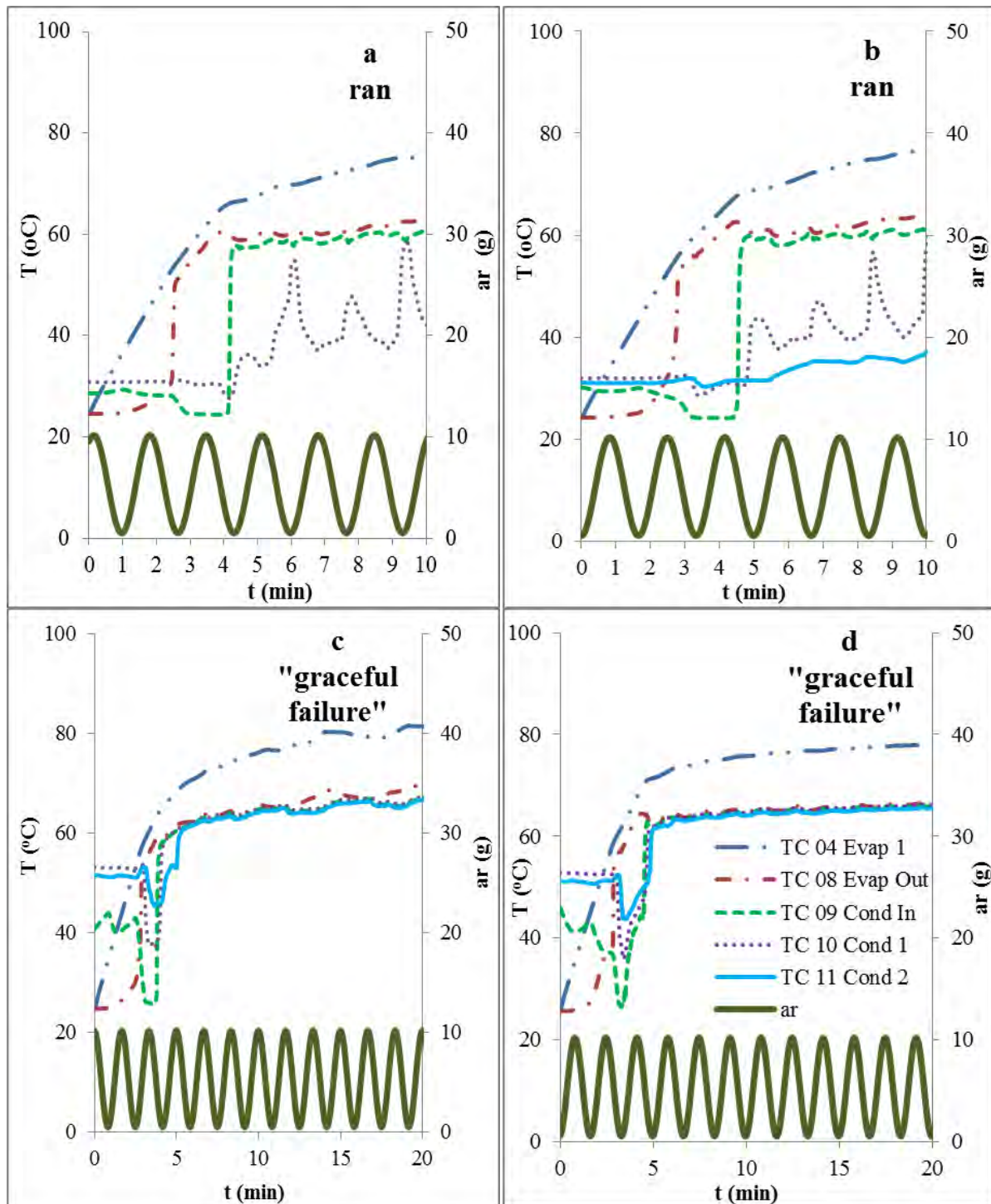


Figure 15. Mode II transient loop heat pipe response for a step input evaporator heat rate,  $Q_{in} = 300\text{W}$ , with a steady-periodic radial acceleration, in the form of a sine wave, with frequency,  $f = 0.01\text{Hz}$ , and peak-to-peak amplitude,  $0.5g \leq a_r \leq 10g$ , for (a) the heat input started at max acceleration and  $T_{cp} = 30^\circ\text{C}$ , (b) the heat input started at min acceleration and  $T_{cp} = 30^\circ\text{C}$ , (c) the heat input started at max acceleration and  $T_{cp} = 52^\circ\text{C}$ , and (d) the heat input started at min acceleration and  $T_{cp} = 50^\circ\text{C}$ .

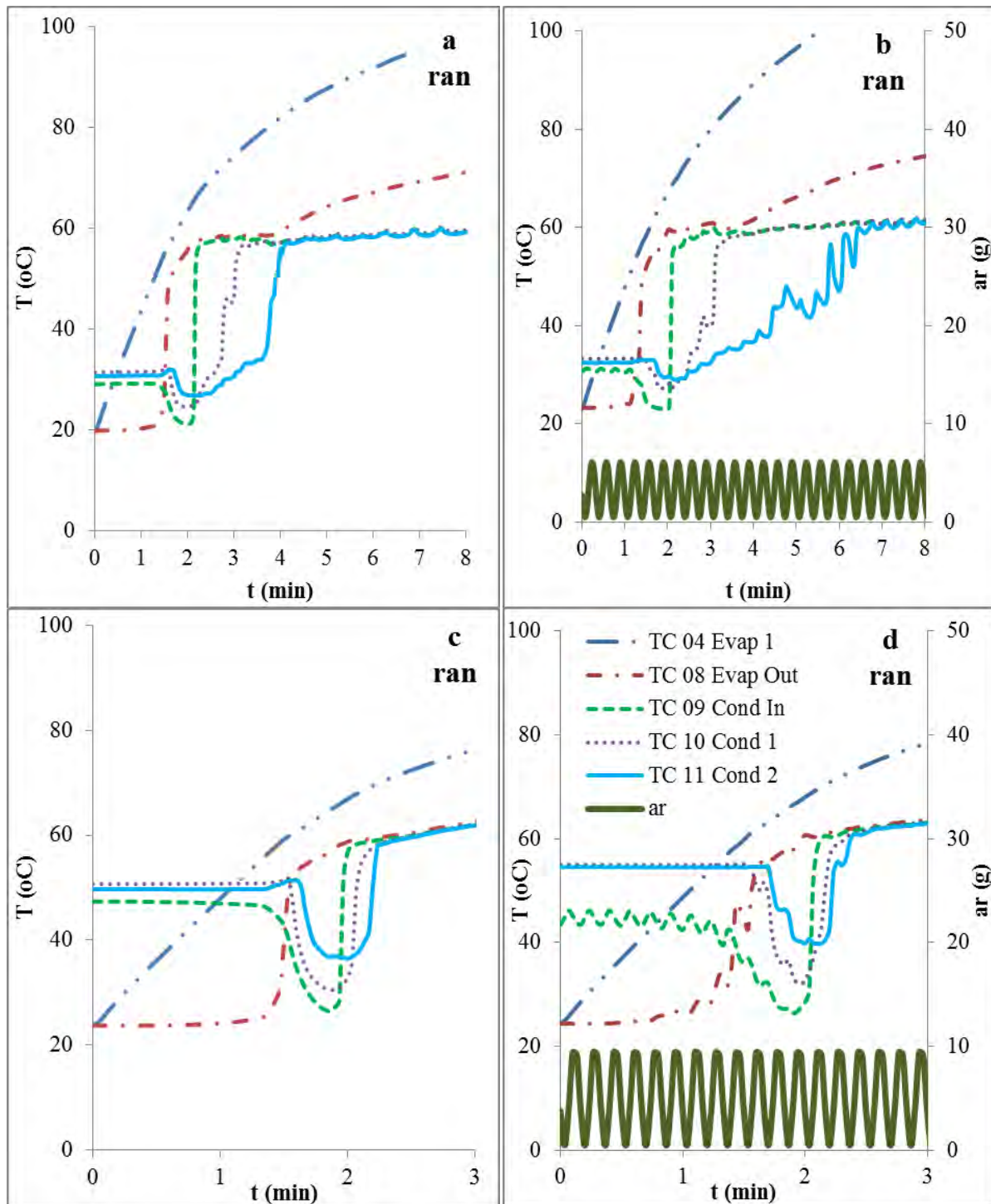


Figure 16. Transient loop heat pipe response for an evaporator heat rate to (a) a step input evaporator heat rate,  $Q_{in} = 600W$ , no acceleration and  $T_{cp} = 30^\circ C$ , (b) a steady-periodic radial acceleration, sine wave, with frequency,  $f = 0.05Hz$  with peak-to-peak amplitude,  $0.5g \leq a_r \leq 10g$  at steady-state conditions for  $Q_{in} = 600W$  and  $T_{cp} = 32^\circ C$ , (c) a step input evaporator heat rate,  $Q_{in} = 600W$ , no acceleration and  $T_{cp} = 50^\circ C$ , and (d) a steady-periodic radial acceleration, sine wave, with frequency,  $f = 0.1Hz$  with peak-to-peak amplitude,  $0.5g \leq a_r \leq 10g$  at steady-state conditions for  $Q_{in} = 600W$  and  $T_{cp} = 52^\circ C$ .



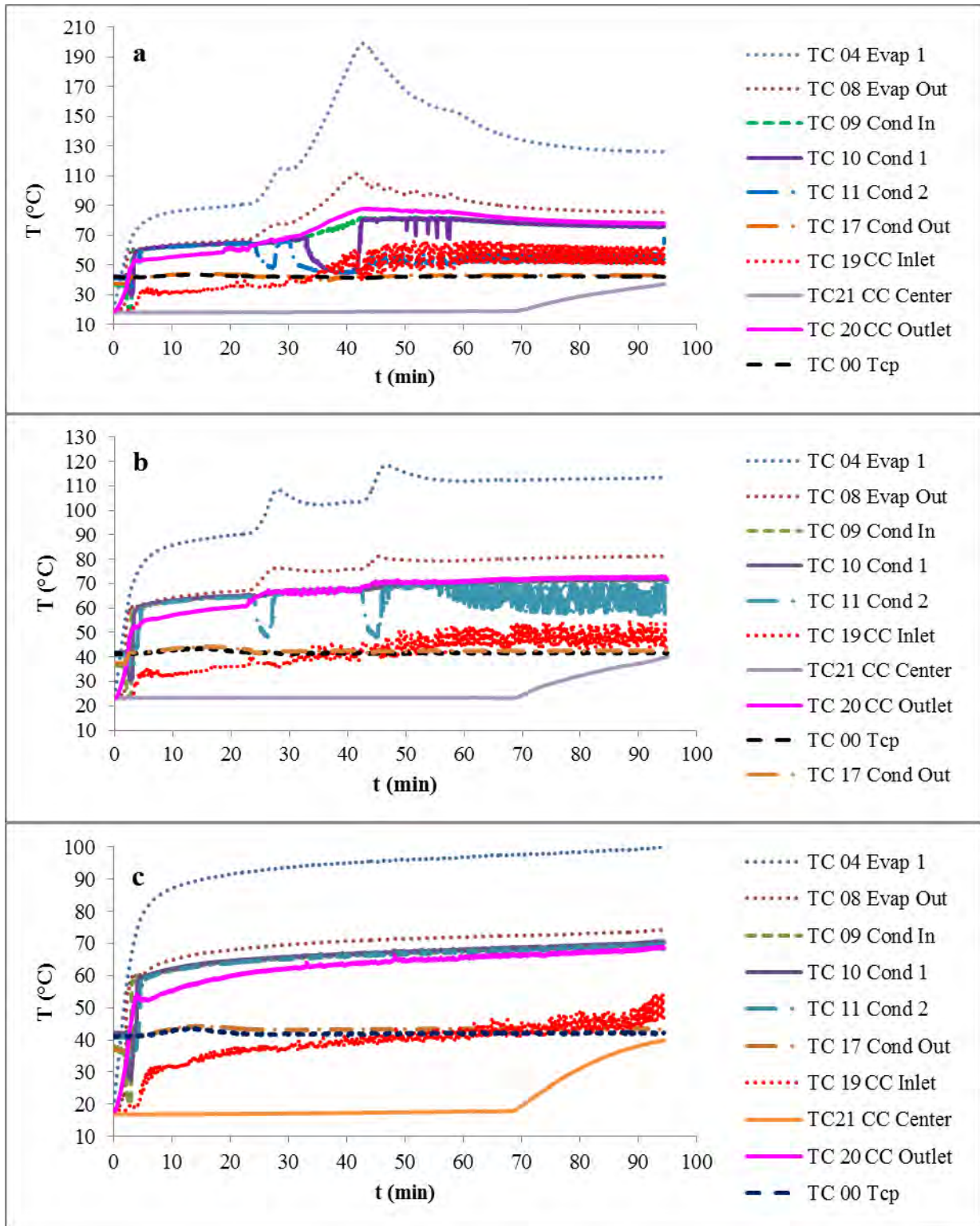


Figure 17. Extended transient loop heat pipe response due to a variation in the minimum radial acceleration,  $ar_{min}$ , at  $f = 0.055\text{Hz}$  and  $ar_{max} = 7g$  with a step input evaporator heat rate,  $Q_{in} = 450\text{W}$ , and cold plate inlet temperature,  $T_{cp} = 42^\circ\text{C}$ , for (a)  $ar_{min} = 1.5g$ , (b)  $ar_{min} = 1.0g$ , and (c)  $ar_{min} = 0.5g$ .

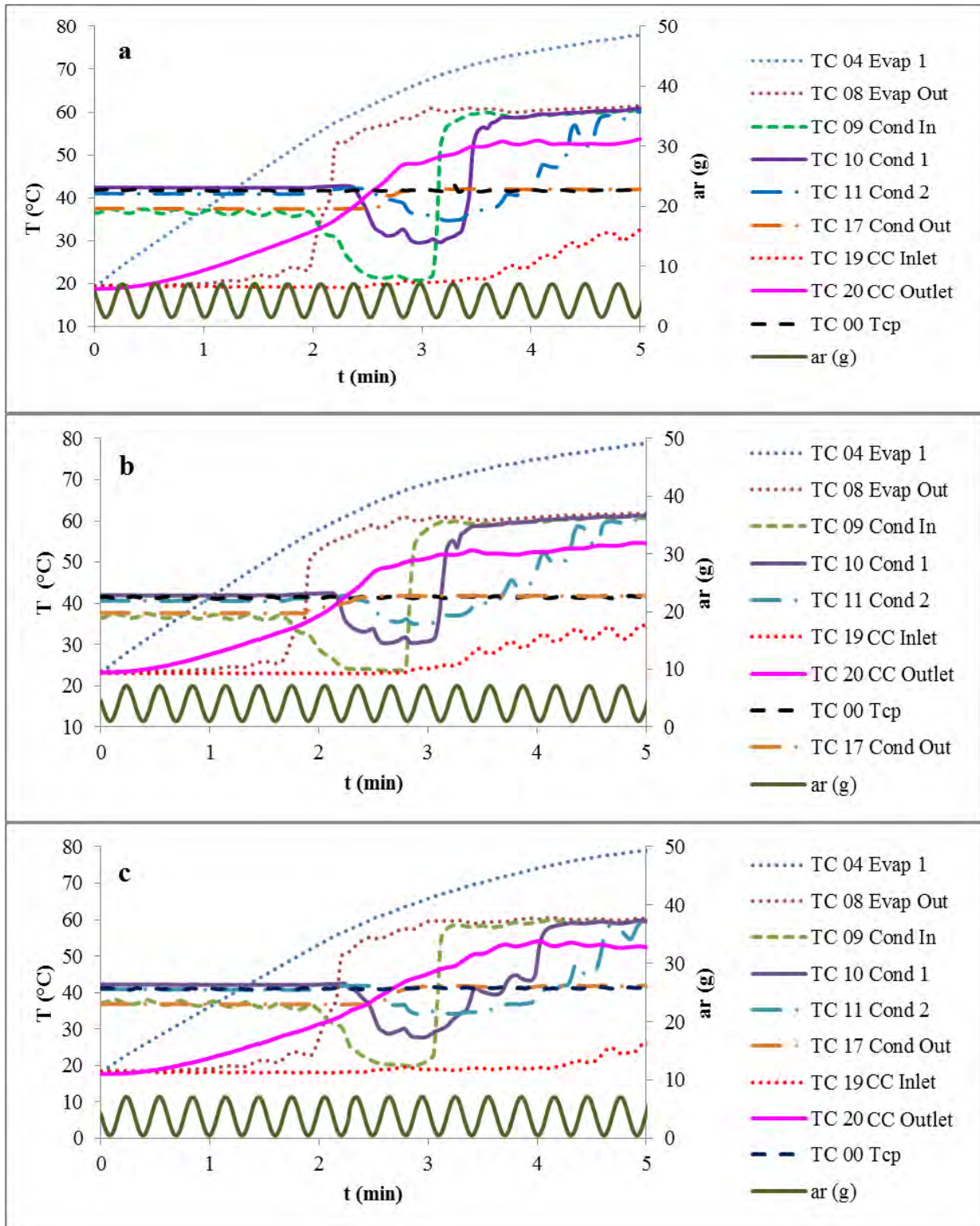


Figure 18. Initial transient loop heat pipe response to a variation in the minimum radial acceleration,  $ar_{min}$ , at  $f = 0.055\text{Hz}$  and  $ar_{max} = 7g$  with a step input evaporator heat rate,  $Q_{in} = 450\text{W}$ , and cold plate inlet temperature,  $T_{cp} = 42^\circ\text{C}$ , for (a)  $ar_{min} = 1.5g$ , (b)  $ar_{min} = 1.0g$ , and (c)  $ar_{min} = 0.5g$ .

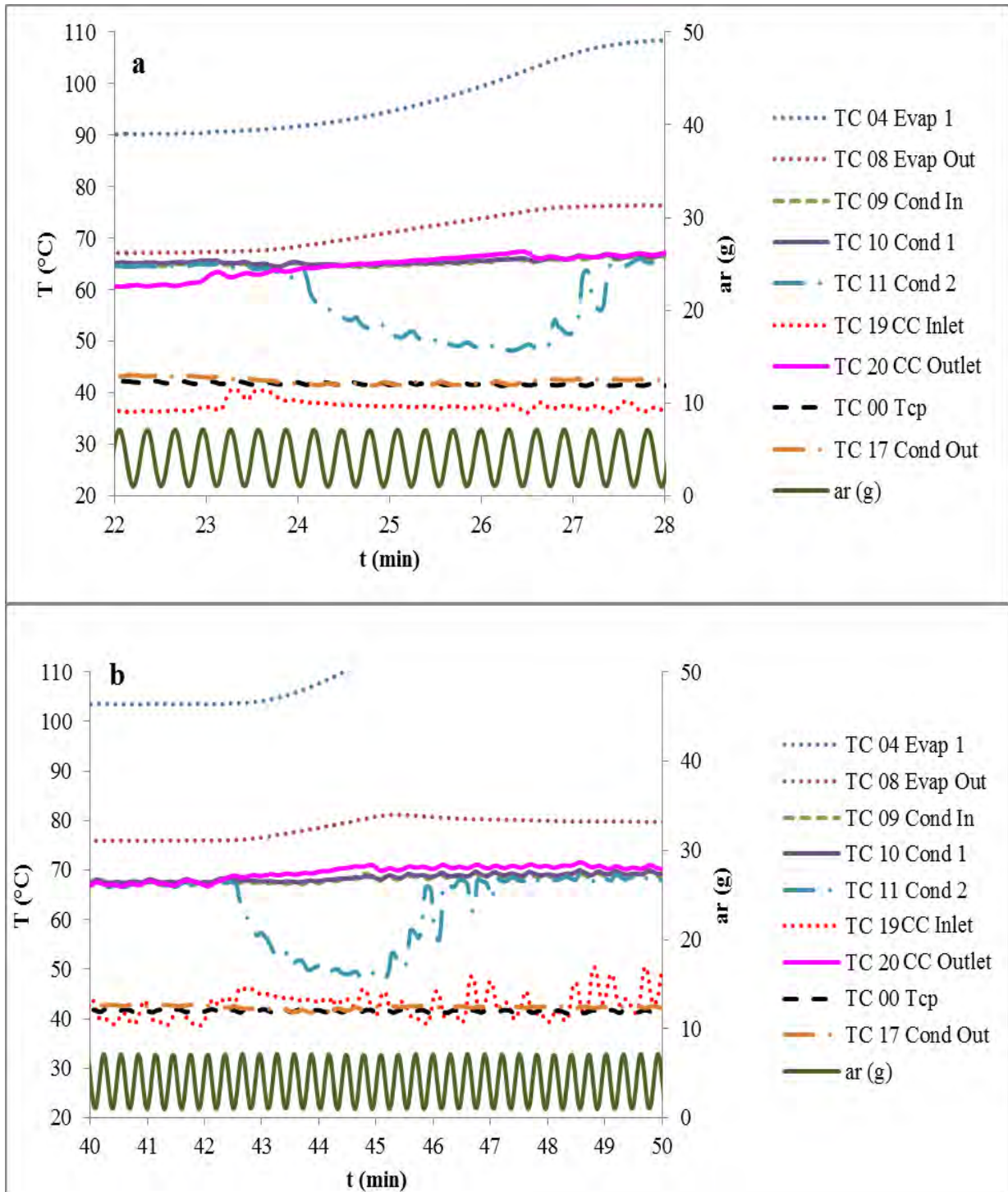


Figure 19. Acceleration driven transients resulting for  $ar_{min} = 1.0g$  leading to a transitory, partial condenser shutdown.



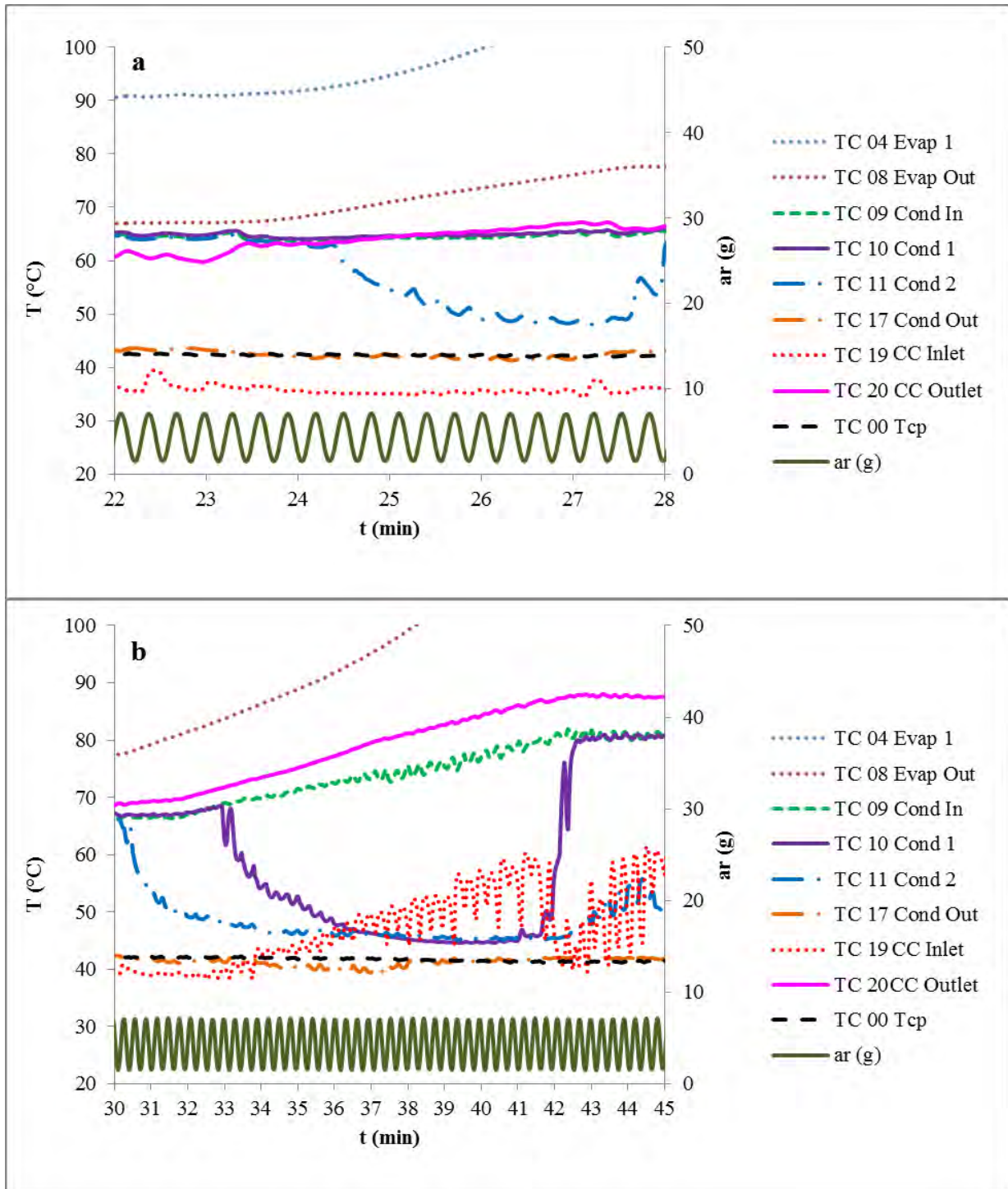


Figure 20. Acceleration driven transients resulting for  $ar_{min} = 1.5g$  leading to a permanent, partial condenser shutdown.

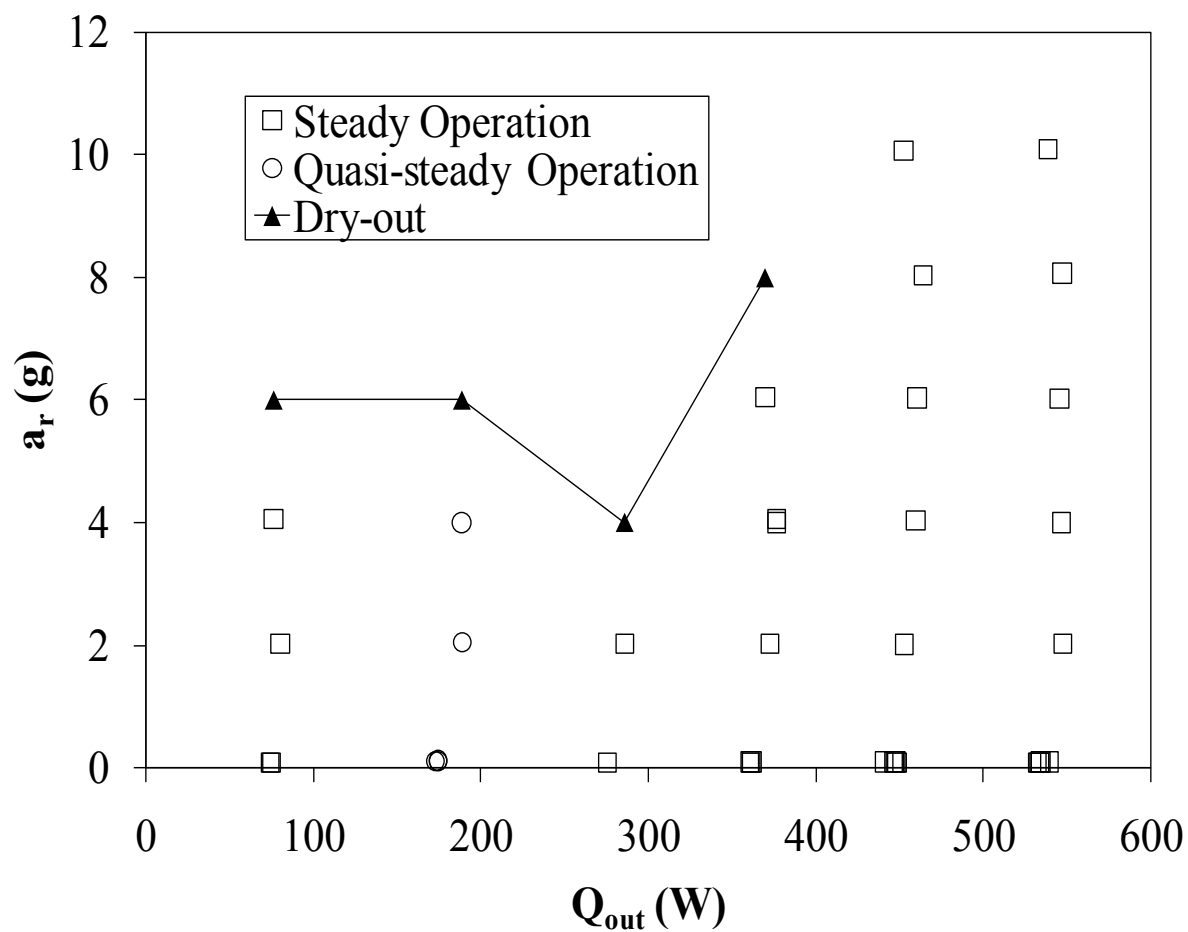


Figure 21. Steady-state performance map of the LHP relating radial acceleration and heat transported by Fleming et al.<sup>10</sup>